

Theory of paramagnetic scattering in highly frustrated magnets with long-range dipole-dipole interactions: the case of 111 Ising pyrochlore systems

Matthew Enjalran^{1*} and Michel J.P. Gingras^{1,2†}

¹*Department of Physics, University of Waterloo, Ontario, N2L 3G1, Canada*

²*Canadian Institute for Advanced Research, 180 Dundas Street West, Toronto, Ontario, M5G 1Z8, Canada*

(Dated: January 27, 2019)

We report results from mean-field theory calculations of the paramagnetic elastic neutron scattering in highly frustrated magnetic systems with long-range dipole-dipole interactions, focusing on the topological $\langle 111 \rangle$ Ising pyrochlore systems ($\text{Ho}_2\text{Ti}_2\text{O}_7$, $\text{Dy}_2\text{Ti}_2\text{O}_7$, $\text{Tb}_2\text{Ti}_2\text{O}_7$). In the spin ice materials ($\text{Ho}_2\text{Ti}_2\text{O}_7$ and $\text{Dy}_2\text{Ti}_2\text{O}_7$), we study the effect of the dipolar Hamiltonian on the paramagnetic spin correlations as a function of the increased range over which the dipole-dipole interaction is summed. Finite range interactions are approximated by direct lattice sums up to an imposed dipole-dipole cut-off distance, denoted r_c (henceforth measured in units of the nearest neighbor distance). The true long-ranged nature of the dipolar interaction is simulated by the Ewald method, $r_c \rightarrow \infty$. We find nearest neighbor spin ice correlations when $r_c = 1$ and observe r_c dependent scattering intensity at finite cut-off distances, $r_c \lesssim 100$. At larger cut-off distances, $r_c \gtrsim 250$, our mean-field results for the paramagnetic scattering agree with the dipolar spin ice description of $\text{Ho}_2\text{Ti}_2\text{O}_7$. In the limit $r_c \rightarrow \infty$ a quasi-degenerate eigen manifold is recovered with an ordering wave vector $\mathbf{q}_{\text{ord}} = (001)$. The mean-field \mathbf{q}_{ord} and predicted spin structure agree with previous Monte Carlo results for a dipolar spin ice model. Modeling $\text{Tb}_2\text{Ti}_2\text{O}_7$ as an antiferromagnetic $\langle 111 \rangle$ Ising pyrochlore, we find that the mean-field paramagnetic scattering is inconsistent with the experimentally observed results. Through simple symmetry arguments we demonstrate that the observed paramagnetic correlations in $\text{Tb}_2\text{Ti}_2\text{O}_7$ are precluded from being generated by $\langle 111 \rangle$ Ising spins but are qualitatively consistent with Heisenberg like moments. Explicit calculations of the paramagnetic scattering pattern for both $\langle 111 \rangle$ Ising and Heisenberg models support these claims. We offer suggestions for reconciling the need to restore spin isotropy with the Ising like structure suggested by the single-ion properties of Tb^{3+} .

PACS numbers: 75.10.Hk, 75.25.+z, 75.30.Gw, 75.40.Cx

I. INTRODUCTION

The pyrochlore oxides, with general formula ($\text{A}_2\text{B}_2\text{O}_7$), have attracted a great deal of attention over the last decade because the combination of lattice geometry and chemical composition allow for a plethora of interesting physical phenomena in these materials^{1,2,3}. The A and B sites on the pyrochlore lattice reside on two distinct inter-penetrating networks of corner sharing tetrahedra, Fig. 1. Since A^{3+} can be either a magnetic rare-earth or a non-magnetic transition metal, and B^{4+} can be a transition metal with or without a moment, there are numerous possibilities to study insulating and itinerant magnetic models in a geometrically frustrated environment. Experimentally, long-range magnetic ordered states^{4,5,6}, novel magnetic phases (e.g., spin glass^{7,8,9,10,11}, spin ice^{3,12,13,14}, spin liquid¹⁵), anomalous Hall effect¹⁶, metallic properties¹⁷, and superconductivity^{18,19} have been observed in the pyrochlore oxides. Materials with the pyrochlore-related spinel structure have also attracted much attention recently. Heavy fermion physics has been observed in the d -electron LiV_2O_4 compound²⁰. In the spinel antiferromagnet ZnCr_2F_4 , a novel spin-Peierls-like transition has been observed²¹ at low temperatures and a protectorate of weakly interacting spin directors slightly above the spin-Peierls transition temperature²².

Our interest resides in insulating rare-earth magnetic

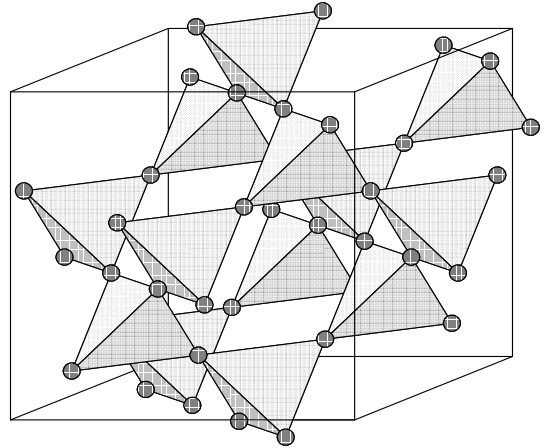


FIG. 1: The pyrochlore lattice structure. The lattice is constructed from a network of corner sharing tetrahedra in which each tetrahedron resides at an fcc Bravais lattice point. A cubic cell contains 4 tetrahedra or 16 atoms.

pyrochlores. In materials of interest to us, rare-earth ions have large dipole moments, i.e., $\mu \gg 1\mu_B$ and small Heisenberg exchange interactions. Hence we ex-

pect long-range dipole-dipole interactions to be a significant contribution to the Hamiltonian. A strong single-ion anisotropy interaction is also present in the systems we study. In particular, the crystal fields produce an effective Ising doublet in the rare-earth ion, A^{3+} . An energy gap separates the ground state doublet from the lowest lying excited states and the Ising quantization axis coincides with the local cubic $\langle 111 \rangle$ direction^{23,24}, i.e., the quantization axis points toward the center of the tetrahedral basis unit cell. This $\langle 111 \rangle$ Ising axis is responsible for endowing frustration to the pyrochlore lattice in the presence of effective nearest neighbor ferromagnetic (FM) interactions^{12,25,26}. From a statistical mechanics point of view, a FM $\langle 111 \rangle$ Ising pyrochlore model is equivalent to a model for disordered water ice, I_h , where both magnetic¹² and water ice^{27,28,29} models possess macroscopic degeneracy. Recent experiments on the magnetic systems $Dy_2Ti_2O_7$ ¹³ and $Ho_2Ti_2O_7$ ^{30,31}, so called spin ice materials, reveal a residual entropy in agreement with the prediction for water ice²⁹. In contrast, nearest neighbor antiferromagnetic (AFM) interactions in a $\langle 111 \rangle$ Ising pyrochlore model are non-frustrated^{24,25,26,32}; therefore, such a model is expected to order at a temperature set by the nearest neighbor energy scale, i.e., $T_N \approx J_{nn}^{eff}/k_B$. A candidate AFM $\langle 111 \rangle$ pyrochlore material is $Tb_2Ti_2O_7$, where a long-range ordered Néel state is expected at $T_N \approx 1$ K^{24,33}. However, experiments indicate the material fails to order down to $T = 70$ mK¹⁵.

On the theoretical end, Monte Carlo (MC) investigations of a $\langle 111 \rangle$ Ising pyrochlore model^{30,33,34} have confirmed the importance of long-range dipolar interactions to the establishment of a spin ice state with a macroscopic entropy that agrees with Pauling's value for the disordered state of water ice²⁹, and with experiments on $Dy_2Ti_2O_7$ ¹³ and $Ho_2Ti_2O_7$ ³⁰. The spin ice spin-spin correlations observed in neutron scattering experiments on $Ho_2Ti_2O_7$ have also been explained by this same dipolar spin ice model³⁰. A general phase diagram involving only the nearest neighbor exchange and dipole energies (T vs J_{nn}/D_{nn}) for dipolar $\langle 111 \rangle$ Ising pyrochlores has been developed³³, and on the spin ice side, $J_{nn}/D_{nn} \geq -0.908$, a long-ranged ordered state, $\mathbf{q}_{ord} = (001)$, is found via loop MC simulations for $T/D_{nn} \lesssim 0.08$ ³⁵, where D_{nn} is the magnetic dipolar energy scale for nearest neighbor Ising moments. Mean-field theory (MFT) has been used to investigate the effects of long-range dipolar interactions in spin ice systems and their inefficiency at lifting the degeneracy established by the nearest neighbor spin ice model^{36,37}. Insights drawn from MFT indicate that perturbations arising from long-range (beyond nearest neighbor) dipolar interactions are themselves frustrated and, therefore, only weakly constrain the system by deforming the free energy landscape into a quasi-degenerate manifold³⁶. It was also observed that if the dipolar sum is not carried out to sufficiently large separation distances, then anomalous ordering can occur. The scenarios described here as well as the role played by the long-range dipoles in the creation of a spin ice phase in $Ho_2Ti_2O_7$

and $Dy_2Ti_2O_7$ and the inhibition of any type of ordering has been disputed by other groups^{14,38,39}. In this context, our aim is to show by direct calculations of the structure factor, $S(\mathbf{q})$, an experimentally measurable quantity, that truncating the interaction range of magnetic dipole-dipole interactions gives rise to a $S(\mathbf{q})$ that severely disagrees at the qualitative level with experimental neutron scattering results on real spin ice materials.

In early theoretical work on $Tb_2Ti_2O_7$, a $\langle 111 \rangle$ model was assumed and a non-collinear Néel state was predicted at $T \approx 1$ K^{24,33}. However, muon spin relaxation measurements indicate a dynamically fluctuating state at all experimentally achievable temperatures, which recent results pushed down below 50 mK⁴⁰. In contrast, recent static susceptibility data suggest a spin glass state at these temperatures⁴¹. In $Tb_2Ti_2O_7$, the energy gap between the ground state doublet and the first excited state doublet is $\Delta \approx 20$ K. The size of anisotropy gap here is an order of magnitude smaller than what is observed in the spin ice materials, $\Delta = 250 - 350$ K, and is comparable to θ_{CW} for $Tb_2Ti_2O_7$. Hence, one might suspect that thermal fluctuations between the ground state and first excited state doublets could restore some spin isotropy in the paramagnetic regime, i.e. $T \gtrsim 5$ K. Several experimental groups have used simple Heisenberg type models (which for the pyrochlore lattice is paramagnetic down to $T \rightarrow 0^+$ ^{42,43,44}) to obtain qualitative agreement with the observed paramagnetic (PM) scattering pattern^{45,46}. Recently, a more detailed calculation using the random phase approximation (RPA) finds that fluctuations out of the Tb^{3+} ground state doublet provides an accurate semi-quantitative picture of the PM correlations⁴⁷.

In this article, we use MFT to investigate the paramagnetic spin-spin correlations of a $\langle 111 \rangle$ Ising dipolar model pertinent to the spin ice materials and $Tb_2Ti_2O_7$. In MFT, the PM regime is realized for temperatures above an energy scale set by the mean-field (MF) critical mode, i.e., $T > T_c^{MF} \equiv \lambda_c^{MF}$, where T is temperature in units of k_B and λ_c^{MF} represents the mean-field global maximum eigenvalue of the \mathbf{q} -dependent susceptibility. As the temperature approaches T_c^{MF} , one expects the critical mode to control the spin-spin correlations. A clear understanding of this critical mode softening relies on an accurate treatment of all interactions in the Hamiltonian. The long-range dipole-dipole interactions are our main concern. The major results from our work are as follows: For the spin ice materials, we demonstrate that imposing an arbitrary cut-off on the range of the dipole-dipole interactions leads to qualitatively incorrect spin-spin correlations in the PM regime and that spin ice correlations are fully recovered in the limit of infinite range dipolar interactions (achieved by use of the Ewald summation technique). In this limit, a true quasi-degenerate and regularized (smooth) free energy landscape results. We predict an ordering wave vector $\mathbf{q}_{ord} = (001)$ in agreement with earlier MC results³⁵, where a two component order parameter soft mode spectrum indicates a spin ice, two-in two-out, moment structure. In the case of ter-

bium titanate, we establish on symmetry grounds and through calculations that the observed PM neutron scattering is inconsistent with a local $\langle 111 \rangle$ Ising dipolar model. Calculations performed for an anisotropic Heisenberg pyrochlore model yield qualitative agreement with experiment and thus support the claim that at least a partial restoration of spin isotropy occurs in $\text{Tb}_2\text{Ti}_2\text{O}_7$. Our MFT results are discussed in the context of the recent results from a random phase approximation (RPA) treatment of $\text{Tb}_2\text{Ti}_2\text{O}_7$ ⁴⁷.

We also have in mind a broader perspective in presenting the enclosed work and detailed derivation of the mean-field formulation of the structure factor, $S(\mathbf{q})$, for highly frustrated magnets. In the past few years, there have been a number of interesting and puzzling thermodynamic data and neutron scattering results on highly frustrated magnets. We briefly discuss some of the systems we are alluding to. One very paradoxical system is the antiferromagnetic $\text{Gd}_3\text{Ga}_5\text{O}_{12}$ garnet (referred to as GGG). This material, where Gd^{3+} is the magnetic ion with a spin $S = 7/2$, consists of two sublattices of intertwined spirals of corner-sharing triangles. For classical Heisenberg spins coupled by nearest-neighbor antiferromagnetic exchange, each spiral on a garnet lattice structure should display a thermally-induced spin-nematic order-by-disorder transition according to work by Moessner and Chalker⁴⁸. In GGG, however, dipolar interactions are approximately 50% of the strength of the exchange interactions for nearest neighbors and is consequently a sizable perturbation to contend with in this system⁴⁹. In zero applied magnetic field, specific heat, magnetic susceptibility and nonlinear susceptibility measurements on GGG strongly suggest that this material undergoes a spin glass transition around 140 mK^{50,51}. However, the nonlinear susceptibility, χ_{nl} , measurements indicate that the spin glass transition in this material is unusual in that χ_{nl} exhibits two maxima⁵¹. However, neutron scattering experiments on powder samples of isotopically enriched ¹⁶⁰Gd (natural Gd has a huge neutron absorption cross-section) indicates the development of spin-spin correlations at approximately 140 mK, extending to a length scale of $\sim 100\text{\AA}$ ^{52,53}. It is unclear at present whether or not the development of extended spin correlations in GGG at ~ 140 mK is an intrinsic effect or is due to material impurities and/or defects⁵⁴. Another interesting system is the $\text{Gd}_2\text{Ti}_2\text{O}_7$ pyrochlore antiferromagnet, where there too Gd^{3+} is the moment-carrying species. In $\text{Gd}_2\text{Ti}_2\text{O}_7$, the dipolar interactions are approximately 20% of the strength of the exchange interactions for nearest neighbors and is here, just as in GGG above, an important perturbation^{4,5,55}. Palmer and Chalker argue that the ground state consists of a fully ordered structure where each tetrahedral unit cell has an identical (zero total magnetic moment) spin configuration (a so-called $\mathbf{q}_{\text{ord}} = (000)$ structure)⁵. However, recent experiments on $\text{Gd}_2\text{Ti}_2\text{O}_7$ are rather puzzling and appear inconsistent with Palmer and Chalker's work. Specifically, neutron diffraction measurements on

¹⁶⁰Gd isotopically enriched powders find a partially ordered phase with one disordered sublattice and propagation vector $\mathbf{q} = (\frac{1}{2}\frac{1}{2}\frac{1}{2})$ at $T = 50$ mK⁶, hence incompatible with the predictions of Palmer and Chalker⁵. Specific heat measurements find strong evidence for two transitions at $T = 0.7$ K and at $T = 1.0$ K⁵⁵. So for $\text{Gd}_2\text{Ti}_2\text{O}_7$, there too exists a complex behavior as signaled by thermodynamic measurements, theoretical predictions and neutron scattering results. Finally, the $\text{Yb}_2\text{Ti}_2\text{O}_7$ pyrochlore ferromagnet is also puzzling⁵⁶. There, neutron scattering results, muon spin relaxation and Mössbauer experiments suggest a ground-state which lacks long-range magnetic order while there exist good evidence from the Mössbauer data that a first order spin freezing transition occurs around $T_f \sim 0.24$ K. Meanwhile, elastic neutron scattering results reveal the development of nontrivial spin-spin correlations as T_f is approached from above. In this system too, it is possible that long range dipolar interactions play an important role due to the contribution of the $|J, m_J\rangle = |7/2, \pm 7/2\rangle$ eigenstate within the effective $S_{\text{eff}} = 1/2$ ground state doublet⁵⁶. All the experimental results we have reviewed above raise a common issue: To further our current understanding in a number of highly frustrated magnets, we need to have a clear and quantitative understanding of the predominant correlations that initially develop out of the paramagnetic state as the materials are cooled. The mean-field theory described herein is a first approach to formulate such program. For concreteness, this paper focuses on the specific cases of insulating pyrochlore oxides with local $\langle 111 \rangle$ Ising moments. It is straightforward to use the formalism herein to tackle the frustrated dipolar systems described above in this paragraph as well as others.

The outline of the paper is as follows: In Section II a condensed description of the MFT formalism of neutron scattering for the anisotropic Heisenberg and $\langle 111 \rangle$ Ising pyrochlores is presented. We give the MFT results for the paramagnetic scattering of the spin ice materials and terbium titanate in Section III. Section IV focuses on the comparison with experiments and emphasizes the point that spin ice physics depends on the recovery of a quasi-degenerate free energy landscape, which is achieved only through an accurate treatment of the long-range dipolar interactions. The need to relax the $\langle 111 \rangle$ Ising constraint to allow for transverse fluctuations in the case of $\text{Tb}_2\text{Ti}_2\text{O}_7$ is discussed in Section IV. For completeness, we include several detailed appendices. In Appendix A, the variational MFT is discussed and the equations for elastic neutron scattering are derived in detail. An alternate approach, a high temperature series expansion, to the equations for neutron scattering is presented in Appendix B. The derivation of the Ewald equations for the \mathbf{q} -dependent dipole-dipole Hamiltonian is given in Appendix C. Appendix D contains a detailed discussion of the symmetry allowed scattering patterns for $\langle 111 \rangle$ Ising and Heisenberg pyrochlores. We note that other authors have discussed various aspects of the mean-field theory^{43,57,58,59,60} and Ewald^{61,62,63,64} derivations pre-

sented in Appendices A and C, respectively. Our purpose here is to provide a self-contained reference for the application of the Ewald method within a mean-field formalism, connecting at times results from earlier work⁵⁹, that will be useful to other researchers who wish to study frustrated magnetic systems with non-Bravais lattice geometries and allowing for an array of possible spin symmetries.

II. MEAN FIELD THEORY OF NEUTRON SCATTERING IN THE PYROCHLORES

In this section, we present the models and provide an outline of the derivation of the mean-field equations for the neutron scattering cross-section, $d\sigma(Q)/d\Omega$, for classical spins on the pyrochlore lattice. The resulting equations are only applicable in the disordered, paramagnetic, regime of the model Hamiltonians. Our focus is on $\langle 111 \rangle$ Ising pyrochlores, but we employ the more general anisotropic Heisenberg model throughout our presentation in order to appeal to a wider body of systems. Mention of specific $\langle 111 \rangle$ results is made at several key points in the MF derivation. The anisotropic model is also of importance here because of its relevance to our discussion of $\text{Tb}_2\text{Ti}_2\text{O}_7$. Our method is best described as variational mean-field theory⁵⁷ (VMFT) (which is equivalent to a Gaussian approximation of the free energy) and has been used to study frustrated magnetic systems^{43,59,60}. The details of VMFT and its application to the scattering cross-section are presented in Appendix A. The use of MFT here to tackle a highly degenerate system with discrete spins, like spin ice, may be considered inappropriate by some. Hence, we provide an alternate interpretation in which the correlations $\langle \mathbf{S}(0) \cdot \mathbf{S}(r) \rangle$ are correctly treated to order $\beta = 1/T$ (or $\chi(\mathbf{q})$ to $1/T^2$) in MFT. This is demonstrated in Appendix B, where scattering cross-section equations are derived via a high temperature series expansion.

A. Models

The pyrochlore lattice, Fig. 1, is a non-Bravais lattice which we describe as a fcc lattice with a four atom unit cell. The positions of the fcc Bravais lattice points, which coincide with a corner point on the tetrahedral basis, are denoted by \mathbf{R}_i . The four atoms that form the tetrahedron at each fcc point (and represent different sublattices) are labeled by \mathbf{r}^a . Hence, the position of a site in the pyrochlore lattice is given by $\mathbf{R}_i^a = \mathbf{R}_i + \mathbf{r}^a$. Table I lists our convention for the tetrahedral basis coordinates, \mathbf{r}^a . The most general Hamiltonian for rare-earth spins on the pyrochlore lattice is a Heisenberg model with nearest neighbor exchange, dipole-dipole, and single-ion

anisotropy (with a local $\langle 111 \rangle$ orientation) energies,

$$H_H = -J \sum_{\langle(i,a),(j,b)\rangle} \mathbf{S}_i^a \cdot \mathbf{S}_j^b - \Delta \sum_{i,a} (\hat{z}^a \cdot \mathbf{S}_i^a)^2 \quad (1)$$

$$+ D_{\text{dd}} \sum_{(i,a)>(j,b)} \left(\frac{\mathbf{S}_i^a \cdot \mathbf{S}_j^b}{|\mathbf{R}_{ij}^{ab}|^3} - \frac{3(\mathbf{S}_i^a \cdot \mathbf{R}_{ij}^{ab})(\mathbf{S}_j^b \cdot \mathbf{R}_{ij}^{ab})}{|\mathbf{R}_{ij}^{ab}|^5} \right).$$

The unit vector \hat{z}^a represents the local $\langle 111 \rangle$ quantization axis that points toward the center of a tetrahedron. Table I defines our convention for \hat{z}^a . The spins \mathbf{S}_i^a have unit length and full $O(3)$ symmetry, \mathbf{R}_{ij}^{ab} is the vector separation between spins \mathbf{S}_i^a and \mathbf{S}_j^b , and J and Δ define the exchange and single-ion energy scales, respectively. The convention established in Eq. 1 defines $J > 0$ as FM and $J < 0$ as AFM exchange energies. The dipolar energy scale is set by $D_{\text{dd}} \equiv DR_{\text{nn}}^3$, where

$$D = \frac{\mu_o \mu^2}{4\pi R_{\text{nn}}^3},$$

μ is the moment on the rare-earth ion, and R_{nn} is the nearest neighbor distance.

The $\langle 111 \rangle$ Ising dipolar model for the pyrochlore lattice³³ is obtained by considering the limit of large Ising anisotropy in Eq. 1 ($\Delta/|J| \gg 1$ and $\Delta/D \gg 1$). The low energy physics of this system is modeled by the Hamiltonian,

$$H_I = -J \sum_{\langle(i,a),(j,b)\rangle} (\hat{z}^a \cdot \hat{z}^b) \sigma_i^a \sigma_j^b \quad (2)$$

$$+ D_{\text{dd}} \sum_{(i,a)>(j,b)} \left(\frac{(\hat{z}^a \cdot \hat{z}^b)}{|\mathbf{R}_{ij}^{ab}|^3} - \frac{3(\hat{z}^a \cdot \mathbf{R}_{ij}^{ab})(\hat{z}^b \cdot \mathbf{R}_{ij}^{ab})}{|\mathbf{R}_{ij}^{ab}|^5} \right) \sigma_i^a \sigma_j^b$$

By low energy physics we mean that the single-ion term in Eq. 1 is removed and the spins are restricted to lie along the local $\langle 111 \rangle$ quantization axis, i.e., $\mathbf{S}_i^a = \hat{z}^a \sigma_i^a$ with $\sigma_i^a \pm 1$. If one were to truncate the dipolar sum in Eq. 2 at nearest neighbor distances, then the following effective nearest neighbor energy scale could be defined,

$$J_{\text{nn}}^{\text{eff}} \equiv J_{\text{nn}} + D_{\text{nn}} = \frac{J}{3} + \frac{5D}{3}. \quad (3)$$

For FM effective nearest neighbor exchange, $J_{\text{nn}}^{\text{eff}} > 0$, one has the nearest neighbor spin ice model of Harris *et al.*, Refs. 12 and 25. If the nearest neighbor interactions $J_{\text{nn}}^{\text{eff}}$ are AFM, then the model possesses a unique ordered state ($\mathbf{Q} = \mathbf{0}$, all-in all-out Néel state) at temperatures on the order of $|J_{\text{nn}}^{\text{eff}}|^{24,25,26,32}$. The transition between the spin ice and $\mathbf{Q} = \mathbf{0}$ phases occurs at $J_{\text{nn}}/D_{\text{nn}} = -1.0$. When dipole-dipole sum is extended to long-range distances, the transition between the $\mathbf{Q} = \mathbf{0}$ and the spin ice states shifts to $J_{\text{nn}}/D_{\text{nn}} \cong -0.908$. Hence, long-range dipolar interactions favor the AFM phase slightly³³.

B. Mean-field theory

We are interested in calculating the elastic neutron scattering cross-section for both Heisenberg and $\langle 111 \rangle$

TABLE I: Our convention for vectors: The \mathbf{r}^a define the basis vectors and \hat{z}^a define the local $\langle 111 \rangle$ anisotropy axes for spins on the pyrochlore lattice. The size of the corresponding cubic cell is given by \bar{a} and contains 16 atoms. Vectors \hat{n}^u represent the global Cartesian basis vectors.

$\mathbf{r}^{(1)}$	$\frac{\bar{a}}{4}(0,0,0)$	$\hat{z}^{(1)}$	$\frac{1}{\sqrt{3}}(1,1,1)$	$\hat{n}^{(1)}$	$(1,0,0)$
$\mathbf{r}^{(2)}$	$\frac{\bar{a}}{4}(1,1,0)$	$\hat{z}^{(2)}$	$\frac{1}{\sqrt{3}}(-1,-1,1)$	$\hat{n}^{(2)}$	$(0,1,0)$
$\mathbf{r}^{(3)}$	$\frac{\bar{a}}{4}(1,0,1)$	$\hat{z}^{(3)}$	$\frac{1}{\sqrt{3}}(-1,1,-1)$	$\hat{n}^{(3)}$	$(0,0,1)$
$\mathbf{r}^{(4)}$	$\frac{\bar{a}}{4}(0,1,1)$	$\hat{z}^{(4)}$	$\frac{1}{\sqrt{3}}(1,-1,-1)$		

Ising spins on the pyrochlore lattice at the mean-field level. Therefore, we use the general anisotropic Hamiltonian, H_H , as the starting point for MFT and include a local, fictitious field term, $|\mathbf{h}| = |\mathbf{h}_i^a|$, (where at the end of the calculation $\mathbf{h}_i^a \rightarrow \mathbf{0}$),

$$H_H = -\frac{1}{2} \sum_{i,j} \sum_{a,b} \sum_{u,v} \mathcal{J}_{uv}^{ab}(i,j) S_i^{a,u} S_j^{b,v} - \sum_{i,a,u} h_i^{a,u} S_i^{a,u}, \quad (4)$$

where

$$\begin{aligned} \mathcal{J}_{uv}^{ab}(i,j) = & J \delta_{\mathbf{R}_{ij}^{ab}, \mathbf{R}_{nn}} (\hat{n}^u \cdot \hat{n}^v) \\ & + \Delta \delta_{i,j} \delta^{a,b} (\hat{z}^a \cdot \hat{n}^u) (\hat{z}^b \cdot \hat{n}^v) \\ & - D_{dd} \left(\frac{(\hat{n}^u \cdot \hat{n}^v)}{|\mathbf{R}_{ij}^{ab}|^3} - \frac{3(\hat{n}^u \cdot \mathbf{R}_{ij}^{ab})(\hat{n}^v \cdot \mathbf{R}_{ij}^{ab})}{|\mathbf{R}_{ij}^{ab}|^5} \right). \end{aligned} \quad (5)$$

In the notation of this general model, the spin vectors are represented by $\mathbf{S}_i^a = \hat{n}^{(1)} S_i^{a,1} + \hat{n}^{(2)} S_i^{a,2} + \hat{n}^{(3)} S_i^{a,3}$, where the unit vectors \hat{n}^u are the global Cartesian unit vectors, see Table I, and $S_i^{a,u}$ is the u -th component of spin. For $\langle 111 \rangle$ Ising spins, one begins with H_I , Eq. 2, and adds the field term $-\sum_{i,a} (\mathbf{h}_i^a \cdot \hat{z}^a) \sigma_i^a$. The resultant interaction parameter, $\mathcal{J}^{ab}(i,j)$, does not include the spin components.

The general expression for the mean-field free energy is as follows,

$$\begin{aligned} F_\rho = & \text{Tr}\{\rho H_H\} + T \text{Tr}\{\rho \ln \rho\} \\ = & \langle H_H \rangle_\rho + T \langle \ln \rho \rangle_\rho, \end{aligned} \quad (6)$$

where ρ is the many-body density matrix and Tr represents a trace over the states of ρ . A mean-field form for F_ρ is obtained by first expressing the many-body density matrix as a product of single-particle density matrices $\rho(\{\mathbf{S}_i^a\}) = \prod_{i,a} \rho_i^a(\mathbf{S}_i^a)$, followed by minimizing F_ρ with respect to ρ_i^a (the variational parameters) subject to the constraints $\text{Tr}\{\rho_i^a\} = 1$ and $\text{Tr}\{\rho_i^a \mathbf{S}_i^a\} = \mathbf{m}_i^a$, where \mathbf{m}_i^a is the local, vector order parameter. For Ising spins, \mathbf{m}_i^a has only one component, m_i^a . Next, the resulting mean-field free energy is transformed to momentum space by applying the definitions,

$$m_i^{a,u} = \sum_{\mathbf{q}} m_{\mathbf{q}}^{a,u} e^{-i\mathbf{q} \cdot \mathbf{R}_i^a}, \quad (7)$$

$$\mathcal{J}_{uv}^{ab}(i,j) = \frac{1}{N_{\text{cell}}} \sum_{\mathbf{q}} \mathcal{J}_{uv}^{ab}(\mathbf{q}) e^{i\mathbf{q} \cdot \mathbf{R}_{ij}^{ab}}, \quad (8)$$

where N_{cell} is the number of fcc Bravais lattice points. We note that the above convention for the Fourier transform, which employs the position of the spin, \mathbf{R}_i^a , results in a real symmetric \mathbf{q} -dependent interaction matrix $\mathcal{J}(\mathbf{q})$, 12×12 for Heisenberg and 4×4 for Ising spins. An alternate convention for the Fourier transform uses \mathbf{R}_i , the Bravais lattice points, instead of \mathbf{R}_i^a and yields a complex $\mathcal{J}(\mathbf{q})$, refer to Appendix A for details. For a non-Bravais lattice, the interaction matrix is not fully diagonalized by a Fourier transform. Hence, to completely diagonalize $\mathcal{J}(\mathbf{q})$ one must transform the \mathbf{q} -dependent variables, $\mathbf{m}_{\mathbf{q}}^a$, to normal mode variables. In component form, the normal mode transformation is given by

$$m_{\mathbf{q}}^{a,u} = \sum_{\alpha=1}^4 \sum_{\mu=1}^3 U_{u,\mu}^{a,\alpha}(\mathbf{q}) \phi_{\mathbf{q}}^{\alpha,\mu}, \quad (9)$$

where the indices (α, μ) label the normal modes (12 for Heisenberg spins), and $\{\phi_{\mathbf{q}}^{\alpha,\mu}\}$ are the amplitudes of the normal modes. In matrix form, $U(\mathbf{q})$ is the unitary matrix that diagonalizes $\mathcal{J}(\mathbf{q})$ in the sublattice space with eigenvalues $\lambda(\mathbf{q})$. Hence, $U_{u,\mu}^{a,\alpha}(\mathbf{q})$ represents the (a, u) component of the (α, μ) eigenvector at \mathbf{q} with eigenvalue $\lambda_{\mu}^{\alpha}(\mathbf{q})$. Finally, the mean-field free energy to quadratic order in the normal modes reads,

$$\mathcal{F}_\rho(T) = \frac{1}{2} \sum_{\mathbf{q}, \alpha, \mu} (nT - \lambda_{\mu}^{\alpha}(\mathbf{q})) |\phi_{\mathbf{q}}^{\alpha,\mu}|^2 - T \sum_{\mathbf{q}, \alpha, \mu} \tilde{h}_{\mathbf{q}}^{\alpha,\mu} \phi_{\mathbf{q}}^{\alpha,\mu}, \quad (10)$$

where $\mathcal{F}_\rho(T) = F_\rho(T)/N_{\text{cell}}$, $\tilde{h}_{\mathbf{q}}^{\alpha,\mu} \propto \mathbf{h}_{\mathbf{q}}^{a,u}/T$, T is the temperature in units of k_B , and $n = 3$ for Heisenberg spins. Note that for the Ising case, the indices u and μ are dropped from Eq. 10 and $n = 1$. We have also dropped a constant from the expression for $\mathcal{F}_\rho(T)$, refer to Appendix A.

The neutron scattering cross-section for unpolarized neutrons in the dipole approximation is given by the general expression^{65,66},

$$\frac{d\sigma(Q)}{d\Omega} = C [f(Q)]^2 \sum_{i,j} \sum_{a,b} \langle \mathbf{S}_{i\perp}^a \cdot \mathbf{S}_{j\perp}^b \rangle e^{i\mathbf{Q} \cdot \mathbf{R}_{ij}^{ab}}, \quad (11)$$

where \mathbf{Q} is the momentum transfer, $\mathbf{Q} = \mathbf{G} + \mathbf{q}$, \mathbf{G} is a reciprocal lattice vector and \mathbf{q} is a vector in the first zone, $f(Q)$ is the magnetic form factor of the relevant scattering ion, and C is a constant. The spin-spin correlation function only involves spin components perpendicular to \mathbf{Q} (i.e., $\mathbf{S}_{i\perp}^a = \mathbf{S}_i^a - (\mathbf{S}_i^a \cdot \mathbf{Q})\mathbf{Q}/|\mathbf{Q}|^2$) and can be written as,

$$\begin{aligned} \langle \mathbf{S}_{i\perp}^a \cdot \mathbf{S}_{j\perp}^b \rangle = & \sum_{u,v} (\hat{n}^u \cdot \hat{n}^v - (\hat{n}^u \cdot \hat{Q})(\hat{n}^v \cdot \hat{Q})) \\ & \times \langle S_i^{a,u} S_j^{b,v} \rangle \\ = & \sum_{u,v} \left(\delta^{u,v} - \frac{Q^u Q^v}{|\mathbf{Q}|^2} \right) \langle S_i^{a,u} S_j^{b,v} \rangle \end{aligned} \quad (12)$$

where $\hat{Q} = \mathbf{Q}/|\mathbf{Q}|$. The correlation function $\langle S_i^{a,u} S_j^{b,v} \rangle$ is expressed as a thermal average of the mean-field variables

and then transformed to normal modes,

$$\langle S_i^{a,u} S_j^{b,v} \rangle = \sum_{\mathbf{q}, \mathbf{q}'} \sum_{\alpha, \beta} \sum_{\mu, \nu} \langle \phi_{\mathbf{q}}^{\alpha, \mu} \phi_{\mathbf{q}'}^{\beta, \nu} \rangle U_{u, \mu}^{a, \alpha}(\mathbf{q}) U_{v, \nu}^{b, \beta}(\mathbf{q}') \quad (13)$$

$$\times e^{-i\mathbf{q} \cdot \mathbf{R}_i^a} e^{-i\mathbf{q}' \cdot \mathbf{R}_j^b}.$$

The correlation function of normal mode variables is calculated from derivatives of the mean-field partition function, $Z = \text{Tr}\{e^{-\beta \mathcal{F}_\rho(T)}\}$, where $\mathcal{F}_\rho(T)$ is given by Eq. 10, with respect to $\tilde{h}_{\mathbf{q}}^{\alpha, \mu}$. The result is

$$\langle \phi_{\mathbf{q}}^{\alpha, \mu} \phi_{\mathbf{q}'}^{\beta, \nu} \rangle = \frac{\delta^{\alpha, \beta} \delta^{\mu, \nu} \delta_{\mathbf{q}+\mathbf{q}', 0}}{(3 - \lambda^{\alpha, \mu}(\mathbf{q})/T)}, \quad (14)$$

for Heisenberg spins and

$$\langle \phi_{\mathbf{q}}^{\alpha} \phi_{\mathbf{q}'}^{\beta} \rangle = \frac{\delta^{\alpha, \beta} \delta_{\mathbf{q}+\mathbf{q}', 0}}{(1 - \lambda^{\alpha}(\mathbf{q})/T)}, \quad (15)$$

for $\langle 111 \rangle$ Ising spins.

Using Eqs. 12, 13, and 14 or 15 in Eq. 11 and carrying out the sums, one obtains equations for the scattering cross-section. In the case of Heisenberg spins, we have

$$\frac{1}{N_{\text{cell}}} \frac{d\sigma(Q)}{d\Omega} = C [f(Q)]^2 \sum_{\alpha, \mu} \frac{|\mathbf{F}_{\mu, \perp}^{\alpha}(\mathbf{q})|^2}{(3 - \lambda^{\alpha, \mu}(\mathbf{q})/T)}, \quad (16)$$

where

$$\mathbf{F}_{\mu, \perp}^{\alpha}(\mathbf{q}) = \sum_a \left\{ \mathbf{U}_{\mu}^{a, \alpha}(\mathbf{q}) - (\mathbf{U}_{\mu}^{a, \alpha}(\mathbf{q}) \cdot \hat{Q}) \hat{Q} \right\} e^{i\mathbf{G} \cdot \mathbf{r}^a} \quad (17)$$

is a 3-component vector. For $\langle 111 \rangle$ Ising spins, one has

$$\frac{1}{N_{\text{cell}}} \frac{d\sigma(Q)}{d\Omega} = C [f(Q)]^2 \sum_{\alpha} \frac{|\mathbf{F}_{\perp}^{\alpha}(\mathbf{q})|^2}{(1 - \lambda^{\alpha}(\mathbf{q})/T)}, \quad (18)$$

with

$$\mathbf{F}_{\perp}^{\alpha}(\mathbf{q}) = \sum_a \hat{z}_{\perp}^a U^{a, \alpha}(\mathbf{q}) e^{i\mathbf{G} \cdot \mathbf{r}^a}, \quad (19)$$

where $\mathbf{F}_{\perp}^{\alpha}(\mathbf{q})$ is still a 3-component vector and $\hat{z}_{\perp}^a = \hat{z}^a - (\hat{z}^a \cdot \hat{Q}) \hat{Q}$.

Equations 16 and 18 are the main results of this section. They provide a mean-field description for the PM elastic neutron scattering of Heisenberg and $\langle 111 \rangle$ Ising moments, respectively, on the pyrochlore lattice. The range of temperature of the paramagnetic regime is set by the maximum eigenvalue according to

$$T > T_c^{\text{MF}} \equiv \max_{\mathbf{q}} \{ \lambda^{\max}(\mathbf{q}) \} / n, \quad (20)$$

where $\lambda^{\max}(\mathbf{q})$ is the maximum eigenvalue at wave vector \mathbf{q} , and $\max_{\mathbf{q}}$ selects the global maximum for all \mathbf{q} . The $\max_{\mathbf{q}} \{ \lambda^{\max}(\mathbf{q}) \}$ occurs at the ordering wave vector \mathbf{q}_{ord} .

III. NEUTRON SCATTERING

In this section we present results from our MF calculation of the neutron scattering cross-section, defined by Eqs. 16 and 18, and the underlying eigen spectrum. We begin with results for the Ising spin ice materials. Results for $\text{Tb}_2\text{Ti}_2\text{O}_7$ as a $\langle 111 \rangle$ Ising and an anisotropic Heisenberg system are presented next.

A. Spin ice materials

Within the MFT result for $\langle 111 \rangle$ Ising spins, the neutron scattering cross-section, Eq. 18, is controlled by the eigen modes of $\mathcal{J}(\mathbf{q})$. At high temperatures compared to the mean-field ordering temperature (PM regime), $T > T_c^{\text{MF}}$, see Eq. 20, all modes contribute to the scattering intensity, i.e., all values of \mathbf{q} in Eq. 18 contribute. However, at temperatures very close to T_c^{MF} , the critical mode dominates the scattering profile as the term $T/(T - T_c^{\text{MF}})$ diverges. A MF ordering wave vector is selected from $T_c^{\text{MF}} = \lambda^{\max}(\mathbf{q}_{\text{ord}})$. Therefore, a clear understanding of the developing paramagnetic correlations in these $\langle 111 \rangle$ pyrochlore magnets depends on a careful treatment of interactions in $\mathcal{J}(\mathbf{q})$, where our greatest concern lies with long-range dipolar interactions. Spin ice at nearest neighbor distances has $J_{\text{nn}}^{\text{eff}} > 0$ with $D_{\text{nn}} > |J_{\text{nn}}|$ and produces a completely degenerate eigen spectrum. Interactions beyond nearest neighbor, only long-range dipole-dipole here, produce perturbations on this degenerate manifold that has been argued to lead to the selection of preferred ordering wave vector³⁶. To ensure that any selected state preserves the symmetry of our true long-ranged Hamiltonian, the dipolar sum must be handled with care, i.e., performed to sufficiently large separation distances such that any truncated terms prove negligible to the physics. The r -dependence of the dipole-dipole energy in spin ice is evaluated systematically by imposing a cut-off distance r_c , measured henceforth in units of the nearest neighbor separation, on the lattice sum. We consider r_c cut-off distances as far out as 1000 nearest neighbors in this approach. The Ewald technique is used to extend the interaction distance to infinity. Therefore, we are able to study the development of the spin-spin correlations and underlying soft mode spectrum in a controlled manner as r_c ranges from the nearest neighbor distance to the infinite range limit. A detailed derivation of the Ewald equations in \mathbf{q} -space is provided in Appendix C. Earlier mean-field studies of spin ice focused on the evolution of the soft mode spectrum as one increased the range of the dipolar interactions out to $r_c = 1000$ ^{36,67}. We present some of those results next to provide continuity with our scattering data.

The Fourier transformed dipole energy is given by,

$$\mathcal{A}(\mathbf{q}) = \sum_i' \sum_{a,b} \frac{\hat{z}^a \cdot \hat{z}^b}{|\mathbf{R}_{ij}^{ab}|^3} - \frac{3(\hat{z}^a \cdot \mathbf{R}_{ij}^{ab})(\hat{z}^b \cdot \mathbf{R}_{ij}^{ab})}{|\mathbf{R}_{ij}^{ab}|^5} \times e^{-i\mathbf{q} \cdot \mathbf{R}_{ij}^{ab}}, \quad (21)$$

where \sum_i' means all $\mathbf{R}_{ij}^{ab} = \mathbf{0}$ terms in the sum are excluded. The \mathbf{q} -dependent dipole energy is evaluated at $D_{\text{nn}} > 0$ ($J_{\text{nn}} = 0$) which places the interaction in the spin ice regime³³. $\mathcal{A}(\mathbf{q})$ is a 4×4 matrix and has four eigenvalues, $(\lambda^\alpha(\mathbf{q}), \alpha = 1, 2, 3, 4)$ at each \mathbf{q} point. The soft mode spectrum, $\lambda^{\text{max}}(\mathbf{q})$, is generated for each point in the (hhl) -plane, measured in units of $2\pi/\bar{a}$. At a cut-off distance of $r_c = 1$, the λ^{max} -spectrum is flat with magnitude $\lambda^{\text{max}}(\mathbf{q})/D = 10/3 \equiv 2J_{\text{eff}}/D$, the expected analytic result, see Fig. 2 in Ref. 36. The \mathbf{q} -independent spectrum for the maximum eigenvalues reflects the strong degeneracy of the zero energy modes of nearest neighbor spin ice in real space. As r_c is increased beyond nearest neighbor, a \mathbf{q} -dependent λ^{max} -spectrum appears. The location of $\lambda^{\text{max}}(\mathbf{q}_{\text{ord}})$, the global maximum, moves seemingly unpredictably about the first zone for cut-offs up to $r_c \approx 100$, Figs. 3-5 in Ref. 36. The fluctuations (ripples) in the spectrum are visible over the first zone and are especially strong near the zone origin. At larger cut-off distances, the soft mode spectrum in the (hhl) -plane begins to smooth out and $\lambda^{\text{max}}(\mathbf{q}_{\text{ord}})$ settles near the zone edge point (001), but small fluctuations in the spectrum persist even out to the largest cut-off distance studied, $r_c = 1000$, see Fig. 6 in Ref 36 and Fig. 3 below. It is only when one evaluates $\mathcal{A}(\mathbf{q})$ by the Ewald technique, effectively taking $r_c \rightarrow \infty$, that the manifold of $\lambda^{\text{max}}(\mathbf{q})$ becomes smooth and quasi-degenerate with a global maximum at (001). The values of $\lambda^{\text{max}}(\mathbf{q})/D$ in the Ewald limit are shown in Fig. 2. The discontinuity in the spectrum occurs only at the zone center, $\mathbf{q} = (000)$, and is due to the discontinuous nature of $\mathcal{A}(\mathbf{q})$ as $\mathbf{q} \rightarrow \mathbf{0}$ (see Appendix C). The effect of r_c on the soft mode spectrum of spin ice, summarizing the results of Ref. 36, is clearly demonstrated in a plot of $\lambda^{\text{max}}(\mathbf{q})$ vs \mathbf{q} along (001), see Fig. 3.

The PM neutron scattering in the (hhl) -plane is calculated from Eq. 18. We use input parameters that are appropriate for both $\text{Ho}_2\text{Ti}_2\text{O}_7$ ($J_{\text{nn}} = -0.52\text{K}, D = 2.35\text{K}$) and $\text{Dy}_2\text{Ti}_2\text{O}_7$ ($J_{\text{nn}} = -1.24\text{K}, D = 2.35\text{K}$)³³, we note that for $\langle 111 \rangle$ Ising spins the nearest neighbor energies are rescaled according to $J_{\text{nn}} = J_1/3$ and $D_{\text{nn}} = 5D/3$ because of the local $\langle 111 \rangle$ quantization axes³³. Recall that the MF equation for the scattering cross-section is valid only for $T > T_c^{\text{MF}}$, see Eq. 20. Henceforth, we set T in units of T_c^{MF} .

With the dipolar sum in $\mathcal{J}(\mathbf{q})$ cut-off at $r_c = 1$, we observe strong scattering throughout the first zone and extending beyond along the (001) and (hhh) directions in agreement with results for the nearest neighbor spin ice model³⁰. Once r_c is set beyond nearest neighbor distances, regions of maximum intensity develop inside the first zone, in accordance with the appearance of a

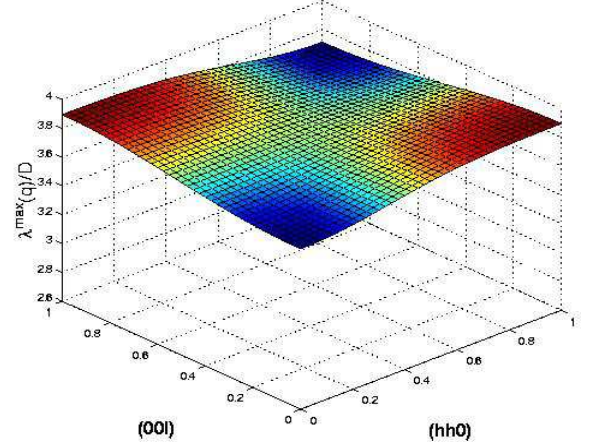


FIG. 2: Maximum eigenvalues for $\mathcal{A}(\mathbf{q})$, the \mathbf{q} -dependent dipole-dipole energy, in the spin ice regime and in the (hhl) -plane, \mathbf{q} is expressed in units of $2\pi/\bar{a}$. The dipoles are treated with the Ewald technique. There is a discontinuity in the spectrum at $\mathbf{q} = \mathbf{0}$ that depends on the direction from which \mathbf{q} approaches zero.

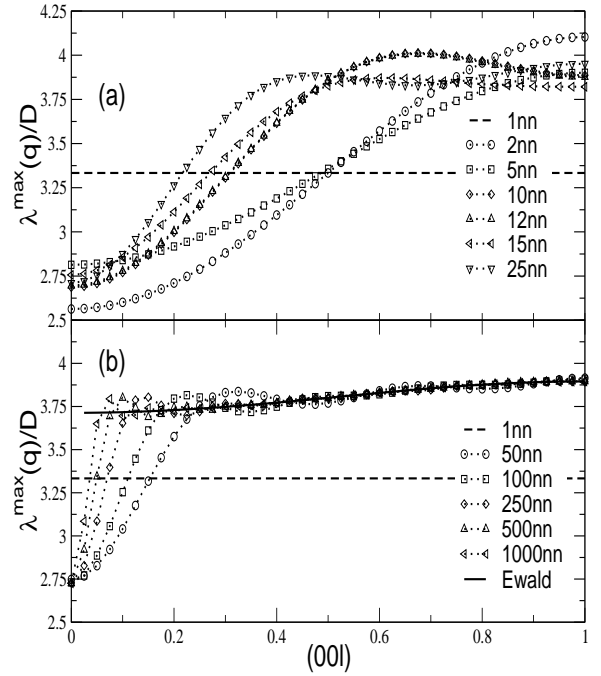


FIG. 3: Maximum eigenvalues for $\mathcal{A}(\mathbf{q})$ along the (001) \mathbf{q} -direction in the spin ice regime for small (a) and large (b) dipolar cut-off distances, r_c . At $r_c = 1$, dashed line, the degenerate nearest neighbor spin ice manifold is produced. The quasi-degenerate eigen spectrum of the dipolar spin ice model is reproduced in the limit of infinite range interactions, which one approaches with $r_c > 1000$ but is achieved by treating the dipole-dipole interactions via the Ewald method, solid line.

global maximum in the λ^{max} -spectrum. Scattering pro-

files for intermediate cut-off distances, $r_c = 5, 10, 15$, at $T = 1.5T_c^{\text{MF}}$, are shown in Fig. 4. The scattering intensity shifts from the corners of the first zone at $r_c = 5$ to incommensurate \mathbf{q} -points for $r_c = 10$ and $r_c = 15$, producing paramagnetic scattering inconsistent with neutron data for $\text{Ho}_2\text{Ti}_2\text{O}_7$ ³⁰ and $\text{Dy}_2\text{Ti}_2\text{O}_7$ ⁶⁸. Maximum PM correlations at incommensurate points in the first zone continue for dipole cut-off distances as large as $r_c \approx 100$.

It has been argued^{14,39} that the physics of spin ice is correctly captured by a model with the long-range dipole-dipole interactions cut-off at finite distances (of the order $r_c \approx 10$). In particular, that the correct ground state is obtained. If the ground state may, in some circumstances, be properly captured at finite r_c , our results for the soft mode spectrum indicate that this is strictly a fortuitous occurrence. For the self-screening property of the dipolar Hamiltonian is accurately treated only in the infinite range limit. In addition, the results in Fig. 4 clearly demonstrate that the qualitative details of the PM scattering depend on the value of r_c ⁶⁹. Since the calculation can be done in the $r_c \rightarrow \infty$ limit with no unnecessary approximations, we consider the discussion of what is happening at finite r_c incidental to the physics of spin ice.

As $T \rightarrow T_c^{\text{MF}}$, a spin ice like scattering pattern, similar to that found experimentally³⁰, begins to develop at larger values of r_c , e.g., $r_c > 100$. In the limit of true long-range dipole-dipole interactions (Ewald limit), the paramagnetic neutron scattering from a model with $\text{Ho}_2\text{Ti}_2\text{O}_7$ parameters takes on the spin ice pattern of the experiments³⁰. The MFT results are given in Fig. 5, where one has maximum intensity at (001) with reduced scattering at the zone edge points (0.75, 0.75, 0). The overall scattering profile, the location of the maximum intensity at (001), the predicted MFT ordering wave vector $\mathbf{q}_{\text{ord}} = (001)$, is in good agreement with the experimental results for $\text{Ho}_2\text{Ti}_2\text{O}_7$ and MC generated results for the dipolar spin ice model³⁰. By comparing the results herein with both experimental and MC results³⁰ for $\text{Ho}_2\text{Ti}_2\text{O}_7$, we conclude that in essence the paramagnetic correlations that develop as temperature drops from $T = \infty$ to T_c^{MF} get frozen in to the ice-rules obeying spin ice state at low temperatures without long range order developing^{30,35,70}.

Inspection of the eigenvectors corresponding to the doubly degenerate maximum eigenvalue, $\lambda^{\text{max}}(001)$, suggests two distinct soft modes at the Gaussian level, where one mode has equal moments on sublattices $a = 1$ and $a = 2$ with sublattices $a = 3$ and $a = 4$ disordered and the second mode is just the converse, see Table II. The order parameters for these two states are just the corresponding normal mode amplitudes, $\phi_{\mathbf{q}_{\text{ord}}}^{\alpha=1}$ and $\phi_{\mathbf{q}_{\text{ord}}}^{\alpha=2}$. Using the $\langle 111 \rangle$ Ising forms of Eqs. 7 and 9, the normal

mode amplitudes are written,

$$\begin{aligned} \phi_{\mathbf{q}}^{\alpha} &= \frac{1}{N_{\text{cell}}} \sum_{i,a} (U^{a,\alpha}(\mathbf{q}))^{-1} m_i^a e^{i\mathbf{q}\cdot\mathbf{r}^a} e^{i\mathbf{q}\cdot\mathbf{R}_i} \quad (22) \\ &= \frac{1}{N_{\text{cell}}} \sum_{i,a} U^{\alpha,a}(-\mathbf{q}) m_i^a e^{i\mathbf{q}\cdot\mathbf{r}^a} e^{i\mathbf{q}\cdot\mathbf{R}_i}. \end{aligned}$$

Substituting the eigenvectors $U^{a,\alpha}(\mathbf{q}_{\text{ord}})$ at $\mathbf{q}_{\text{ord}} = (0, 0, 2\pi/\bar{a})$ from Table II, we have the following order parameters,

$$\phi_{\mathbf{q}_{\text{ord}}}^{\alpha=1} = \frac{1}{N_{\text{cell}}} \sum_i \frac{(-m_i^{a=1} + m_i^{a=2})}{\sqrt{2}} e^{i(2\pi/\bar{a})\hat{z}\cdot\mathbf{R}_i} \quad (23)$$

$$\phi_{\mathbf{q}_{\text{ord}}}^{\alpha=2} = \frac{1}{N_{\text{cell}}} \sum_i \frac{i(-m_i^{a=3} + m_i^{a=4})}{\sqrt{2}} e^{i(2\pi/\bar{a})\hat{z}\cdot\mathbf{R}_i} \quad (24)$$

Equations 23 and 24 do not define a spin ice spin structure because $\phi_{\mathbf{q}_{\text{ord}}}^{\alpha=1}$ and $\phi_{\mathbf{q}_{\text{ord}}}^{\alpha=2}$ do not describe a two-in two-out equal moment structure, a state in which all sites have the same spin magnitude, i.e., $|m_i^a| = m$. Hence, we perform a unitary transformation on the ϕ -variables to obtain a new set of variables (order parameters),

$$\Psi_{\mathbf{q}_{\text{ord}}}^{(1)} = \frac{\phi_{\mathbf{q}_{\text{ord}}}^{\alpha=1} + \phi_{\mathbf{q}_{\text{ord}}}^{\alpha=2}}{\sqrt{2}} \quad (25)$$

and

$$\Psi_{\mathbf{q}_{\text{ord}}}^{(2)} = \frac{\phi_{\mathbf{q}_{\text{ord}}}^{\alpha=1} - \phi_{\mathbf{q}_{\text{ord}}}^{\alpha=2}}{\sqrt{2}}. \quad (26)$$

These new order parameters, $\Psi_{\mathbf{q}_{\text{ord}}}^{(1)}$ and $\Psi_{\mathbf{q}_{\text{ord}}}^{(2)}$, have an equal moment on each sublattice, and in MFT all m_i^a have equal magnitude (with $|m_i^a| = 1$ at $T = 0$). The orientation of ordered moments along the local $\langle 111 \rangle$ axis is given by the signs in front of the m_i^a in Eqs. 23 and 24. Hence, $\Psi_{\mathbf{q}_{\text{ord}}}^{(1)}$ defines a spin structure in which moments on sublattices $a = 1, 3$ point out of and those on sublattices $a = 2, 4$ point in to the unit tetrahedron. The ordered state of $\Psi_{\mathbf{q}_{\text{ord}}}^{(2)}$ has moments on sublattices $a = 3, 4$ flipped. Therefore, Eqs. 25 and 26 represent two equivalent spin ice states at \mathbf{q}_{ord} ⁷¹ that at mean-field (Gaussian) level are the predicted ordered states³⁵. The spin configuration represented by $\Psi_{\mathbf{q}_{\text{ord}}}^{(2)}$ is the structure depicted in Fig. 3 of Ref. 35. When one considers the three symmetry equivalent ordering wave vectors, then there are six degenerate $\Psi_{\mathbf{q}_{\text{ord}}}^m$ to describe the full spin ice structure. In all cases, an ordered spin ice structure has no net moment along the direction of the ordering wave vector, as must be the case for dipole interactions⁷².

We note that only data from calculations with $\text{Ho}_2\text{Ti}_2\text{O}_7$ parameters has been displayed here, but results for a model with $\text{Dy}_2\text{Ti}_2\text{O}_7$ parameters are similar. The long-range nature of the dipoles plays the crucial role in the manifestation of spin ice physics in both $\text{Ho}_2\text{Ti}_2\text{O}_7$ and $\text{Dy}_2\text{Ti}_2\text{O}_7$ as well as in the details of the frozen spin configuration at low temperatures.

TABLE II: The MF critical modes, eigenvalues and eigenvectors, of $\mathcal{J}(\mathbf{q}_{\text{ord}})$ at $\mathbf{q}_{\text{ord}} = (001)$ for spin ice (Ho₂Ti₂O₇ parameters) and with dipolar interactions evaluated by the Ewald method. $\lambda^\alpha(\mathbf{q}_{\text{ord}})/D$ and $U^{a,\alpha}(\mathbf{q}_{\text{ord}})$ are the scaled eigenvalues and normalized eigenvectors, respectively. A two order parameter structure is suggested in the Gaussian approximation. In one order parameter, there are moments on sublattices $a = 1, 2$ but no moments on sublattices $a = 3, 4$. In the second order parameter, the situation is reversed.

α	$\lambda^\alpha(\mathbf{q}_{\text{ord}})/D$	$U^{a,\alpha}(\mathbf{q}_{\text{ord}})$
1	3.1575	$\frac{1}{\sqrt{2}}(-1, 1, 0, 0)$
2	3.1575	$\frac{1}{\sqrt{2}}(0, 0, -1, 1)$

B. Tb₂Ti₂O₇ as a $\langle 111 \rangle$ Ising pyrochlore

In a $\langle 111 \rangle$ Ising description of Tb₂Ti₂O₇, the AFM exchange is enhanced relative to the dipole energy scale compared to the spin ice systems discussed above. For Tb₂Ti₂O₇ we use $J_1 = -2.64$ K and $D = 0.48$ K yielding $J_{\text{nn}}/D_{\text{nn}} = -1.1$ ²⁴, which compares to $J_{\text{nn}}/D_{\text{nn}} = -0.22$ for Ho₂Ti₂O₇ and $J_{\text{nn}}/D_{\text{nn}} = -0.52$ for Dy₂Ti₂O₇. Therefore, at a nearest neighbor cut-off distance, Tb₂Ti₂O₇ is an AFM $\langle 111 \rangle$ pyrochlore that is predicted to develop non-collinear Néel order, with ordering wave vector $\mathbf{q}_{\text{ord}} = (000)$, at $T \approx 1$ K^{24,33}. When infinite range dipoles are included, a $\langle 111 \rangle$ Ising model with $J_{\text{nn}}/D_{\text{nn}} = -1.1$ is still predicted to be a long-ranged AFM³³. Hence, the antiferromagnetic exchange in a $\langle 111 \rangle$ model of Tb₂Ti₂O₇ is sufficiently strong to prevent the perturbations arising from long-range dipolar interactions from changing the critical nature of the model. In contrast to the spin ice problem, here the long-range dipoles are perturbations on a non-degenerate manifold. The counter point to the above model predictions is that experimentally Tb₂Ti₂O₇ remains a collective paramagnetic down to very low temperatures, $T \gtrsim 50$ mK⁴⁰. Recent magnetization data have reported the indication of a spin-glass-like transition around 70 mK⁴¹.

As an initial attempt to explain the physics of Tb₂Ti₂O₇, we investigate the PM correlations within MFT and compare to the experimental results for elastic neutron scattering. Experimental data for elastic neutron scattering in Tb₂Ti₂O₇ are shown in Fig. 6(a). The most intense region of scattering is centered around (002) with reduced correlations extending toward (220) and a scattering minimum at (000). From the pyrochlore lattice structure and the MF formalism, we know that the intensity at (002) is controlled by the eigen modes at (000) but modulated by the phase factor $\exp(i\mathbf{G} \cdot \mathbf{r}^a)$, see Eq. 18. This raises the question as to whether the maximum about (002) could be interpreted as the precursor of a long-range ordered non-collinear Néel state.

We begin by considering $\langle 111 \rangle$ Ising spins on the pyrochlore lattice. The neutron scattering intensity profile is determined by $\mathbf{F}_\perp^\alpha(\mathbf{q})$, Eq. 19, and contains only information on the spin anisotropy via \hat{z}^a and the sym-

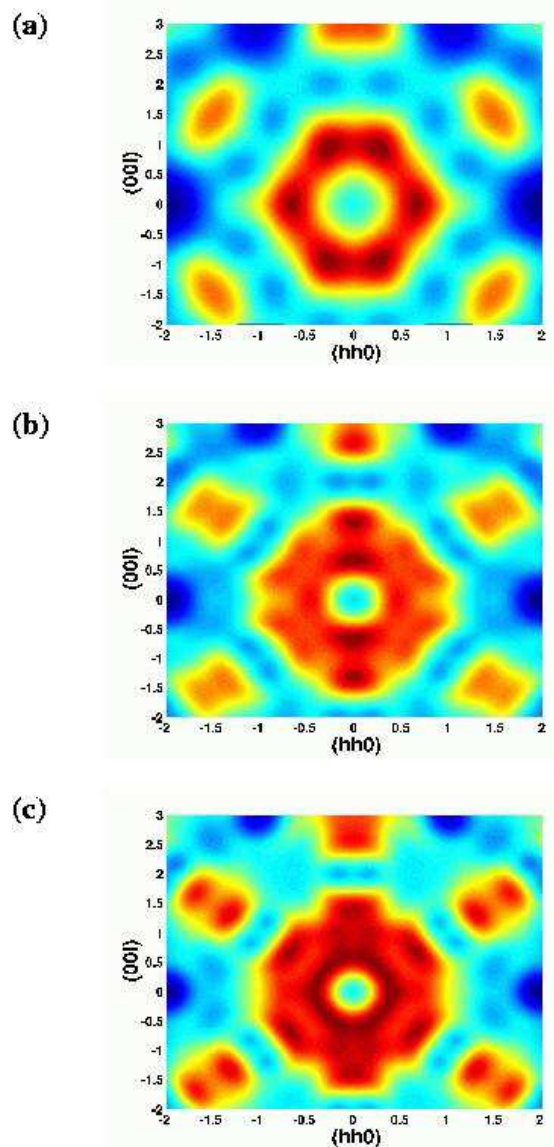


FIG. 4: Paramagnetic scattering in the (hhl) -plane of spin ice (Ho₂Ti₂O₇ parameters and magnetic form factor) as a function of the maximum separation distance in the dipole-dipole sum, r_c , $T = 1.5T_c^{\text{MF}}$ for all scans: (a) $r_c = 5$, (b) $r_c = 10$, (c) $r_c = 15$. Blue denotes regions of minimum scattering intensity while brown marks areas of maximum scattering.

metry of the lattice through the eigenvectors, $U^{a,\alpha}(\mathbf{q})$, and a phase factor, $\exp(i\mathbf{G} \cdot \mathbf{r}^a)$. Hence, the nature and strength of the exchange and dipole-dipole interactions are arbitrary. From these basic symmetry components, we find that $|\mathbf{F}_\perp^\alpha(000)|^2 = |\mathbf{F}_\perp^\alpha(002)|^2$, or that the scattering intensity about (000) and (002) has the same numerical value, disregarding the form factor ($f(Q)$). An equivalent statement is the intensities about (000) and (002) are symmetry related. This strong condition on the scattering pattern is in serious contradiction with the experimentally observed results. In contrast, if we con-

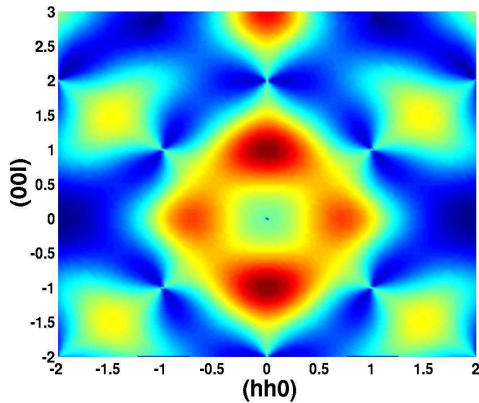


FIG. 5: Paramagnetic scattering in the (hhl) -plane of spin ice ($\text{Ho}_2\text{Ti}_2\text{O}_7$ parameters and magnetic form factor) with dipole-dipole interactions treated via the Ewald technique. Temperature is reduced to $T = 1.17T_c^{\text{MF}}$ to increase contrast. Maximum intensity occurs at (001) .

sider an anisotropic Heisenberg pyrochlore model (Eq. 16 with finite Δ), we find that the lattice and spin degrees of freedom do not force the scattering intensity to be identical about (000) and (002) . For a model with $O(3)$ spin symmetry, the scattering profile is controlled by $\mathbf{F}_\perp^{\alpha,\mu}(\mathbf{q})$, Eq. 17. The significant difference between Eqs. 17 and 19 is the restoration of spin isotropy, i.e., the geometric factor defining the local $\langle 111 \rangle$ quantization axis, \hat{z}^a , is absent from Eq. 17. Therefore, on purely symmetry grounds, no $\langle 111 \rangle$ Ising model for $\text{Tb}_2\text{Ti}_2\text{O}_7$ will reproduce the experimental PM correlations shown in Fig. 6(a). The details upon which our arguments are based are provided in Appendix D. Earlier works have recognized the need to consider more isotropic spin models for $\text{Tb}_2\text{Ti}_2\text{O}_7$. In Ref. 45, the qualitative features of the PM scattering were reproduced from an isotropic structure factor for the near neighbor Heisenberg pyrochlore AFM. Similar results were achieved in Ref. 46 by considering select $\mathbf{Q} = \mathbf{0}$ spin structures on a cluster of two tetrahedra.

To support the picture obtained on symmetry grounds, we have applied our MF formalism to two models for $\text{Tb}_2\text{Ti}_2\text{O}_7$: (1) a pyrochlore system with $\langle 111 \rangle$ Ising spins, and (2) a pyrochlore lattice with Heisenberg spins and finite $\langle 111 \rangle$ anisotropy. In both cases, the dipole-dipole interactions are evaluated with the Ewald method, see Appendix C. For the $\langle 111 \rangle$ Ising description (i.e., $\Delta/|J| \gg 1$ and $\Delta/D \gg 1$ and Eq. 18), we use $J_1 = -2.64\text{K}$ and $D = 0.48\text{K}^{24}$. Our data are shown in Fig. 6(b). Note that the scattering about (000) and (002) is symmetry related, as predicted above, but is an intensity minimum. Monte Carlo data (not shown) for this $\langle 111 \rangle$ model agrees with our MF results. For a Heisenberg model with finite anisotropy (i.e., $\Delta/|J| > 1$ and $\Delta/D > 1$ and Eq. 16), our MF results are provided in Fig 6(c). With an anisotropy strength of $\Delta = 20\text{K}$

(i.e., $\Delta/D \approx 41.7$), we achieve good qualitative agreement with the experiment. The region around (002) has the strongest scattering with reduced intensity near (220) and the interconnecting regions. If we turn off the finite anisotropy ($\Delta = 0$), i.e., an isotropic Heisenberg model with long-range dipoles, the dominate scattering remains about points (002) and (220) , but there is increased intensity along the bridge regions in \mathbf{q} -space connecting these points. If we next treat the dipolar interactions between isotropic moments with a finite cut-off, r_c , then some intensity along the bridge regions at (111) begins to develop, in contrast to the experiments. Finally, in the absence of dipoles one has the near neighbor AFM exchange Heisenberg model, where the scattering intensity forms a network of interconnecting triangles with equal intensity about (002) and (220) ^{45,48,73}. Hence, a restoration of the spin isotropy is sufficient to place scattering about points (002) and (220) in \mathbf{q} -space, but to achieve qualitative agreement with the experimental intensity profile dipolar interactions are necessary as is a finite single-ion contribution to the Hamiltonian.

IV. DISCUSSION

In our mean-field analysis of the $\langle 111 \rangle$ Ising dipolar spin ice model, we are able to study both the PM spin-spin correlations and the \mathbf{q} -dependent eigenvalues as a function of the maximum separation distance, r_c , to which the dipole-dipole interactions are summed. Therefore, in a controlled manner, we can study the symmetry of the dipolar Hamiltonian $A(\mathbf{q})$ as well as its perturbative effect on the spin ice correlations as a function of r_c . Dipolar interactions combine spin and spatial degrees of freedom in a way that produces positive and negative contributions to the total energy. Therefore, dipolar interactions are self-screening, and as one increases the range of interaction one expects the variability in $A(\mathbf{q})$ to induce fluctuations in the soft mode spectrum of spin ice. The potential result of this variability, and one that we observe, is that the MF selected ordering wave vector, \mathbf{q}_{ord} , and the spin-spin correlations, $d\sigma(Q)/d\Omega$, vary with r_c . Because the dipolar sum is only marginally conditionally convergent⁷⁴, i.e., $\sum |\mathbf{R}_{ij}^{ab}|^{-3-\epsilon}$ is absolutely convergent for $\epsilon > 0$, one might expect to achieve satisfactory convergence for some manageable cut-off distance. However, in the case of spin ice, we observed variations in the MF selected \mathbf{q}_{ord} for direct lattice sums even with $r_c = 1000$. It is only by use of the Ewald technique to evaluate dipole-dipole interactions that we effectively damp out any fluctuations and achieve a quasi-degenerate λ^{max} -spectrum with a well defined ordering wave vector, a spin ice moment structure, and PM spin-spin correlations that agree well with MC³⁵ and experimental³⁰ results. We address these points in more detail below.

The perturbations arising from long-ranged dipolar interactions are important for spin ice because they act

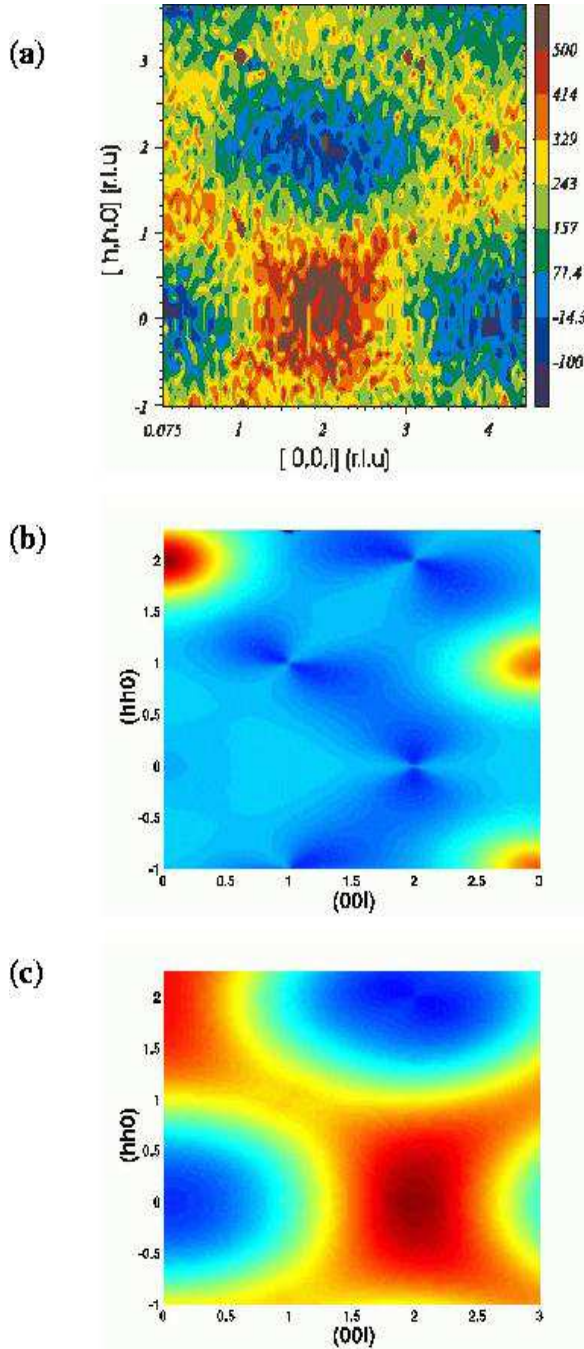


FIG. 6: Paramagnetic scattering in the (hhl) plane for $\text{Tb}_2\text{Ti}_2\text{O}_7$: (a) Experimental paramagnetic scattering⁴⁵ ($T = 9$ K), (b) MF model of $\text{Tb}_2\text{Ti}_2\text{O}_7$ treated as a $\langle 111 \rangle$ Ising pyrochlore ($T = 1.5T_c^{\text{MF}}$), (c) MF model of $\text{Tb}_2\text{Ti}_2\text{O}_7$ treated as an anisotropic Heisenberg pyrochlore ($T = 1.5T_c^{\text{MF}}$, $\Delta = 20$ K).

on the completely degenerate eigenvalue spectrum created at the nearest neighbor level, $r_c = 1$. Hence, as the range of the interaction increases, r_c , the effect of the perturbation on the level structure of the degenerate states may also change in a somewhat a priori un-

predictable manner. As demonstrated in Fig. 4, the calculated PM neutron scattering changes significantly as one increases the maximum range of interaction in $A(\mathbf{q})$ to just beyond the nearest neighbor separation. At distances of $r_c = 5, 10, 15$, the positions of strongest magnetic correlations shift to different regions within the first zone: (i) At $r_c = 5$, $d\sigma/d\Omega|_{\text{max}}$ is at incommensurate points near the zone corners of $\mathbf{q} = (0.275, 0.275, 0.95)$ and $\mathbf{q} = (0.7, 0.7, 0)$; (ii) at $r_c = 10$, $d\sigma/d\Omega|_{\text{max}}$ is inside the zone at $\mathbf{q} = (0, 0, 0.675)$; (iii) at $r_c = 15$, $d\sigma/d\Omega|_{\text{max}}$ is contained within a ring in reciprocal-space at $\mathbf{q} = (0.425, 0.425, 0)$. Again, the PM scattering reflects the underlying soft mode spectrum with maxima at incommensurate \mathbf{q} -points in the first zone. Therefore, at these short dipolar cut-off distances, our $\langle 111 \rangle$ Ising model does not capture an essential feature of the spin ice PM spin-spin correlations that are in qualitative agreement with neutron scattering experiments on $\text{Ho}_2\text{Ti}_2\text{O}_7$ ³⁰. Furthermore, we have found that these arbitrary small cut-offs are responsible for the discrepancy between early Monte Carlo data^{38,39} and experiments on both $\text{Dy}_2\text{Ti}_2\text{O}_7$ and $\text{Ho}_2\text{Ti}_2\text{O}_7$, where agreement was achieved when $r_c \rightarrow \infty$ in $\text{Dy}_2\text{Ti}_2\text{O}_7$ ³³ and $\text{Ho}_2\text{Ti}_2\text{O}_7$ ³⁰. In addition, for small r_c , the predicted MF ordered state, obtained from \mathbf{q}_{ord} and the corresponding eigenvectors $\lambda^{\text{max}}(\mathbf{q}_{\text{ord}})$, is not a two-in two-out structure spin ice, see Table II.

Paramagnetic scattering patterns that differ qualitatively from the observed experimental profile persist out to dipolar cut-off distances of $r_c \gtrsim 100$. Spin ice like scattering begins to appear when the dipolar sum is carried out to distances on the order of 250 nearest neighbors and larger. However, a qualitative glance at the scattering data for large but finite r_c does not reveal the subtle nature of the spin ice state and the importance of the dipolar interactions to its creation. When the Fourier transform of the dipole-dipole interactions, $A(\mathbf{q})$ (See. Appendix C), is calculated for $r_c = 1000$, the PM scattering attains the qualitative features of the experimental and MC results in Ref. 30, i.e., the $r_c = 1000$ results are similar to the Ewald results of Fig. 5. The $\mathbf{q} = (001)$ eigenvalues and eigenvectors at $r_c = 1000$ have the same doubly degenerate, or two soft mode, structure that was observed in the Ewald limit (Table II contains the Ewald results). However, there is an important quantitative difference between the Ewald and $r_c = 1000$ results that a mere glance at $S(\mathbf{q})$ would not reveal, for the $r_c = 1000$ result does not represent the global maximum. At $r_c = 1000$, the value of $\max_{\mathbf{q}}\{\lambda^{\text{max}}(\mathbf{q})\}$ occurs at the nearby point $(0.025, 0.025, 1.0)$, has the value $\lambda^{(1)}(0.025, 0.025, 1.0)/D = 3.1589$, and is *non-degenerate*. The corresponding eigenvector signals a state with a nonzero order parameter on only two of the four sublattices, $(U^{a,1}(0.025, 0.025, 1.0) = (0, 0, 1, -1)/\sqrt{2})$. Hence, while at finite temperatures the PM scattering for a $r_c = 1000$ calculation and an Ewald calculation will appear qualitatively identical, in the limit $T \rightarrow T_c^{\text{MF}}$ the critical correlations are indeed distinct. The level

of discrepancy between these two results is very small, see Fig. 7, but the point is clear for spin ice: The self-screening property of the dipole-dipole interactions does not restore an exact symmetry, and reliable results are achieved only by respecting the true long-range nature of interactions with the Ewald approach.

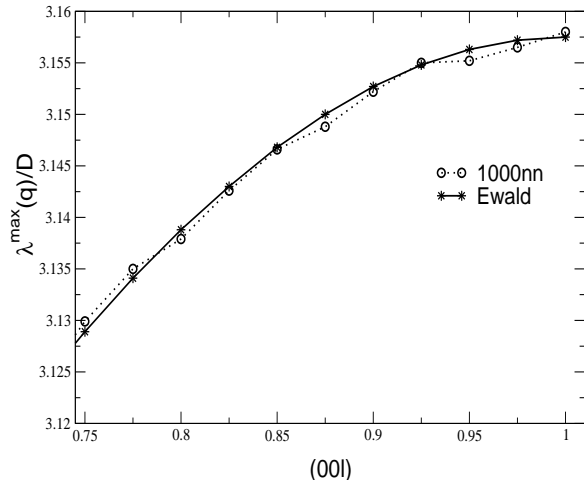


FIG. 7: Maximum eigenvalues along $(00l)$ for spin ice, $\text{Ho}_2\text{Ti}_2\text{O}_7$ parameters, at $r_c = 1000$ and $r_c \rightarrow \infty$, Ewald limit. Deviations between the values of $\lambda^{\max}(\mathbf{q})/D$ for the Ewald treatment and the direct lattice sum out to $r_c = 1000$ are $O(10^{-3})$.

In the case of $\text{Tb}_2\text{Ti}_2\text{O}_7$, the long-ranged dipolar interactions for an appropriate $\langle 111 \rangle$ Ising model do not exert the same control on the energy landscape and PM correlations that we find in spin ice. As mentioned above, this is due to the fact that a $\langle 111 \rangle$ Ising model for $\text{Tb}_2\text{Ti}_2\text{O}_7$ has AFM nearest neighbor interactions that are non-frustrated and yield a well defined unique critical mode. The perturbations on this non-degenerate spectrum produced by the long-ranged dipoles only serve to shift the splitting between non-critical (massive) modes of the various branches. The location of $\lambda^{\max}(\mathbf{q}_{\text{ord}})$ in \mathbf{q} -space does not change. The prediction of this model is an AFM long-range ordered state in which all spins point either in or out of the unit tetrahedra at $T \approx 10^0$ K. However, this prediction is not realized experimentally. Another problem with a $\langle 111 \rangle$ Ising model for $\text{Tb}_2\text{Ti}_2\text{O}_7$, the one we address in this work, is the mean-field PM correlations, see Fig. 6(b), do not agree with the experimentally observed results, Fig. 6(a). In Section III B and in Appendix D, we demonstrated on symmetry grounds alone that no pyrochlore model with $\langle 111 \rangle$ Ising moments could reproduce the basic features of the experimental PM scattering, i.e., strongest intensity centered about (002), lower intensity about (220), and minimum intensity at the zone center (000). These symmetry arguments were also supported by MF and MC calculations of the elastic neutron scattering cross-section, Eq. 18.

In Section III B and in Appendix D, we were also able

to demonstrate on symmetry grounds that a Heisenberg pyrochlore model of $\text{Tb}_2\text{Ti}_2\text{O}_7$ would allow for elastic scattering about (002) while at the same time permit no scattering about (000). A MF calculation of the PM neutron scattering in the (hhl) plane for an anisotropic Heisenberg model with long-range dipoles, Eq. 1, shows good qualitative agreement with the experimental scattering pattern (strongest intensity about (002) with reduced scattering at (220) and along the bridges between these points, see Fig. 6(c)). Both the finite anisotropy ($\Delta/|J| > 1$ and $(\Delta/D > 1)$) and long-range dipoles are necessary to achieve a good qualitative match with the experiments. Reducing either the single-ion anisotropy to the isotropic limit ($\Delta = 0$) or the range of the dipole-dipole interactions in the model reduces this agreement by altering the ratio of scattering intensity between (002) and (220). However, even a model with dipoles cut-off at the first nearest neighbor, $r_c = 1$, improves the picture provided by a nearest neighbor AFM exchange only Heisenberg model presented in Ref. 45. Therefore, a restoration of the spin isotropy is necessary to place paramagnetic scattering about the \mathbf{q} -space points (002) and (220). The dipolar interactions are then important for shifting (i.e. redistributing) the scattering intensity from (220) to (002). Intermediate regions between these two points also experience a reduction in scattering. In terms of the underlying soft-mode spectrum, the $\mathbf{q} = (000)$ eigenvalues and eigenvectors control the scattering at (220) to (002). A shift in intensity from (220) to (002) signals a PM spin structure that prefers to lie in xy -plane (i.e., neutron scattering at (002) comes from spins with components perpendicular to this direction).

Switching to a model with fully isotropic Heisenberg spins (as in Ref. 45) restores all the spin symmetry in the paramagnetic limit. This picture is dramatically inconsistent with the experimentally determined single-ion structure of Tb^{3+} ($J = 6$, 7F_6) in $\text{Tb}_2\text{Ti}_2\text{O}_7$, where a ground state doublet is separated from the first excited doublet by an anisotropy gap of 20 K, close to the θ_{CW} temperature^{23,24}. Therefore, a restoration of the full spin symmetry at $T < 20$ K seems an unlikely explanation for the PM scattering at 9 K.

The current MF approach does not allow the single-ion properties to be systematically considered, but a RPA calculation does⁴⁷. By retaining only the simplest energy level structure in the Tb^{3+} wave function, the ground state doublet and the first excited state doublet, one can relax the strict $\langle 111 \rangle$ Ising constraint on the spins in a controlled approximation. With the RPA, fluctuations out of the ground state and into the first excited state levels are equivalent to a fluctuating canting of spins away from the Ising geometry. In this case, the lowest order fluctuation from the strict $\langle 111 \rangle$ Ising limit yields qualitative agreement with experiment for the paramagnetic spin-spin correlations⁴⁷. Others have also proposed a simple relaxation scheme of the strict $\langle 111 \rangle$ Ising directions⁴⁶. Theoretical work remains to be done to explain the failure of $\text{Tb}_2\text{Ti}_2\text{O}_7$ to order at a tempera-

ture of 1 K, and why it remains paramagnetic down to 50 mK^{15,45}.

V. CONCLUSIONS

In conclusion, we have shown that fluctuations in the free energy landscape of a dipolar spin ice model caused by a finite distance cut-off of the dipole-dipole interactions results in the selection of a critical mode that produces non-spin ice like PM correlations when compared to experimental neutron scattering results. This is observed even if dipolar interactions are summed to a 1000 nearest neighbors. By using the Ewald method, in which the complex dipolar Hamiltonian is summed to the infinite range limit, $r_c \rightarrow \infty$, the artificially introduced fluctuations in the λ^{\max} -spectrum are suppressed and the spin ice ordering wave vector found in MC simulations, (001), is selected. The PM correlations are also in excellent semi-quantitative agreement the experimental and MC results for Ho₂Ti₂O₇, with the maximum intensity at (001), see Fig. 5. The predicted MF ordered state is a structure within the spin ice manifold. We anticipate the selection of a unique spin structure when higher order terms are included in the mean-field free energy as was observed for the Heisenberg pyrochlore Gd₂Ti₂O₇⁵.

For Tb₂Ti₂O₇, we have demonstrated on symmetry grounds, through MF calculations, and MC simulations that the experimentally measured PM elastic neutron scattering is inconsistent with a $\langle 111 \rangle$ Ising pyrochlore spin structure. From the qualitative agreement obtained using an anisotropic Heisenberg model, we argue in favor of a more isotropic effective spin model to describe the low energy phases of Tb₂Ti₂O₇.

Finally, we have demonstrated the usefulness of a combined mean-field theory and Ewald method approach to studying geometrically frustrated magnets with long-range dipole-dipole interactions in the paramagnetic phase. This approach could be applied in general to any geometrically frustrated system. The zero field picture of Gd₃Ga₅O₁₂ (GGG) is particularly interesting because the low temperature phase remains an unresolved issue that entails unraveling the physics of competing exchange and long-range dipole-dipole interactions in a garnet lattice environment^{50,51,52,53,75}.

Acknowledgments

We would like to acknowledge Bill Buyers, Steve Bramwell, Jason Gardner, Bruce Gaulin, Byron den Hertog, Ying-Jer Kao, Roger Melko, Adrian del Maestro, Hamid Molavian, and Jean-Yves Delannoy for many useful discussions. We would also like to thank Adrian del Maestro for a careful reading of the manuscript. This work is supported by NSERC of Canada, Research Corporation and the Province of Ontario.

APPENDIX A: NEUTRON SCATTERING IN THE GAUSSIAN APPROXIMATION

As we noted in the Introduction, other authors have discussed MFT and its application to magnetism^{43,57,58,59,60} and the Ewald method for magnetic dipoles^{62,63,64}. Our purpose is to combine the techniques of MFT, developed here, with the and Ewald procedures for magnetic dipoles in \mathbf{q} -space, developed in Appendix C, so they can be readily applied to other problems of highly frustrated rare-earth magnets.

In this appendix we provide a detailed derivation of the mean-field equations for the elastic scattering cross-section for pyrochlore spin systems. We are particularly interested in the $\langle 111 \rangle$ Ising pyrochlores, but our derivation is performed for Heisenberg spins, with a local $\langle 111 \rangle$ anisotropy, in order to broaden the appeal of the results. Connections to $\langle 111 \rangle$ Ising systems are noted at appropriate points. As mentioned in Section II, the MFT is developed via a variational approach (VMFT), and in general this approach applies to a large array of statistical models with arbitrarily complex order parameters⁵⁷. In this work, the method reproduces the Gaussian approximation (GA) of the Landau free energy. The VMFT described here has been used by others^{43,58,59,60}, and we provide a detailed presentation here to clear up the notational inconsistencies that appeared in some of these previous works. We also wish to provide for comparison with the RPA, which allows for a more controlled relaxation of the $\langle 111 \rangle$ Ising restriction^{47,65} that experimental evidence suggests is needed for Tb₂Ti₂O₇^{45,46}.

We begin with the model Hamiltonian of Eq. 1, H_H . The conventions for the spin vectors, \mathbf{S}_i^a , unit vectors, \hat{n}^u and \hat{z}^a , and the description of the pyrochlore lattice in a rhombohedral basis with a four atom unit cell are as described in Section II. Therefore, our starting Hamiltonian for MFT is given by,

$$H_H = -\frac{1}{2} \sum_{i,j} \sum_{a,b} \sum_{u,v} \mathcal{J}_{uv}^{ab}(i,j) S_i^{a,u} S_j^{b,v} - \sum_{i,a,u} h_i^{a,u} S_i^{a,u}, \quad (\text{A1})$$

where $\mathcal{J}_{uv}^{ab}(i,j)$ is defined by Eq. 5, and a fictitious field term has been added. The field term, with $|\mathbf{h}_i^a| = |\mathbf{h}|$, is removed from the final equations by taking $\mathbf{h}_i^a \rightarrow 0$. We note that indices $(a,b) = 1,2,3,4$ label the sublattices and $(u,v) = 1,2,3$ label the spin components.

In VMFT, an approximate free energy as a function of a trial density matrix, ρ , is formed,

$$F_\rho = \text{Tr}\{\rho H_H\} + T \text{Tr}\{\rho \ln \rho\} = \langle H_H \rangle_\rho + T \langle \ln \rho \rangle_\rho, \quad (\text{A2})$$

where Tr represents a trace over spin variables. F_ρ is variational and defines an upper bound to the actual free energy, i.e., $F_\rho \geq F$. The best functional from for trial density matrix is obtained by minimizing F_ρ with respect to the parameters of ρ . For a system of N particles, the MF form of the N -body density matrix is given by a

product of single particle density matrices,

$$\rho(\{\mathbf{S}_i^a\}) = \prod_{i,a} \rho_i^a(\mathbf{S}_i^a). \quad (\text{A3})$$

The single particle density matrix, ρ_i^a , is treated as a variational parameter that is subject to the constraints

$$\text{Tr}\{\rho_i^a\} = 1, \quad (\text{A4})$$

$$\text{Tr}\{\rho_i^a \mathbf{S}_i^a\} = \mathbf{m}_i^a, \quad (\text{A5})$$

which keep the internal energy constant, i.e., $\text{Tr}\{\rho H\} = C$. Here, \mathbf{m}_i^a is a vector order parameter, for $\langle 111 \rangle$ Ising spins one has the scalar equivalent, $\text{Tr}\{\rho_i^a \sigma_i^a\} = m_i^a$. Incorporating the constraints into the expression for F_ρ gives,

$$\begin{aligned} F_\rho &= \text{Tr}\{\rho H_H\} + T \text{Tr}\{\rho \ln \rho\} \\ &- T \text{Tr}\left\{\sum_{i,a} \xi_i^a (\rho_i^a - 1)\right\} \\ &- T \text{Tr}\left\{\sum_{i,a} (\rho_i^a \mathbf{S}_i^a - \mathbf{m}_i^a) \cdot \mathbf{A}_i^a\right\}, \end{aligned} \quad (\text{A6})$$

where ξ_i^a and \mathbf{A}_i^a are the Lagrange multipliers for the constraints of Eq. A4 and Eq. A5, respectively. In minimizing F_ρ with respect to ρ_i^a , one has the following results,

$$\begin{aligned} \frac{\delta}{\delta \rho_i^a} \text{Tr}\{\rho H_H\} &= 0, \\ \frac{\delta}{\delta \rho_i^a} \text{Tr}\{\rho \ln \rho\} &= \text{Tr}\{\ln \rho_i^a\} + \text{Tr}\{1\}, \\ \frac{\delta}{\delta \rho_i^a} \text{Tr}\left\{\sum_{i,a} \xi_i^a \rho_i^a\right\} &= \text{Tr}\{\xi_i^a\}, \\ \frac{\delta}{\delta \rho_i^a} T \text{Tr}\left\{\sum_{i,a} \rho_i^a \mathbf{S}_i^a \cdot \mathbf{A}_i^a\right\} &= \text{Tr}\{\mathbf{S}_i^a \cdot \mathbf{A}_i^a\}. \end{aligned}$$

The optimum form for the density matrix is found by solving $\delta F_\rho / \delta \rho_i^a = 0$,

$$\rho_i^a = C_i^a e^{\mathbf{A}_i^a \cdot \mathbf{S}_i^a}, \quad (\text{A7})$$

where $C_i^a = e^{\xi_i^a - 1} = 1 / \text{Tr}\{e^{\mathbf{A}_i^a \cdot \mathbf{S}_i^a}\}$ follows from Eq. A4. Evaluating the trace in C_i^a for both Heisenberg and Ising spins we obtain

$$\begin{aligned} \mathcal{Z}_i^a &= \frac{(2\pi)^{3/2}}{(|\mathbf{A}_i^a|)^{1/2}} I_{1/2}(|\mathbf{A}_i^a|) \\ &= \frac{4\pi}{|\mathbf{A}_i^a|} \sinh(|\mathbf{A}_i^a|), \end{aligned} \quad (\text{A8})$$

and

$$\mathcal{Z}_i^a = 2 \cosh(A_i^a), \quad (\text{A9})$$

respectively, where $I_{1/2}(|\mathbf{A}_i^a|)$ is a modified Bessel function. The variational local density matrix is now written as

$$\rho_i^a = \frac{e^{\mathbf{A}_i^a \cdot \mathbf{S}_i^a}}{\mathcal{Z}_i^a} \quad (\text{A10})$$

and is used, along with the constraints of Eqs. A4 and A5, to rewrite the variational free energy,

$$\begin{aligned} F_\rho &= -\frac{1}{2} \sum_{i,j} \sum_{a,b} \sum_{u,v} \mathcal{J}_{uv}^{ab}(i,j) m_i^{a,u} m_j^{b,v} \\ &- \sum_{i,a,u} h_i^{a,u} m_i^{a,u} + T \sum_{i,a} (\mathbf{A}_i^a \cdot \mathbf{m}_i^a - \ln \mathcal{Z}_i^a). \end{aligned} \quad (\text{A11})$$

We want an expression for the free energy to quadratic order in \mathbf{m}_i^a . This means that one must expand $\ln \mathcal{Z}_i^a(\mathbf{A}_i^a)$ and then express \mathbf{A}_i^a as a function of \mathbf{m}_i^a . From the series representation of $\mathcal{Z}_i^a(\mathbf{A}_i^a)$ followed by the series expansion of $\ln(1-x)$, one has

$$\ln \mathcal{Z}_i^a \approx \ln C_1 + \frac{|\mathbf{A}_i^a|^2}{2n}, \quad (\text{A12})$$

where C_1 is a model dependent constant and $n = 1, 3$ for Ising and Heisenberg spins, respectively. Using Eq. A5, one obtains the expression

$$\mathbf{m}_i^a = \hat{A}_i^a \frac{I_{3/2}(|\mathbf{A}_i^a|^2)}{I_{1/2}(|\mathbf{A}_i^a|^2)} \quad (\text{A13})$$

$$= \hat{A}_i^a \left\{ \coth(|\mathbf{A}_i^a|) - \frac{1}{|\mathbf{A}_i^a|} \right\} \quad (\text{A14})$$

for Heisenberg and

$$m_i^a = \tanh(A_i^a) \quad (\text{A15})$$

for Ising spins. To first order, we have

$$\mathbf{m}_i^a = 3\mathbf{A}_i^a, \quad (\text{A16})$$

and

$$m_i^a = A_i^a. \quad (\text{A17})$$

Using Eqs. A12-A17, we can write the MF free energy to quadratic order in the order parameter,

$$\begin{aligned} F_\rho &= \frac{1}{2} \sum_{i,j} \sum_{a,b} \sum_{u,v} m_i^{a,u} \{nT \delta_{i,j} \delta^{a,b} \delta^{u,v} - \mathcal{J}_{uv}^{ab}(i,j)\} m_j^{b,v} \\ &- \sum_{i,a,u} h_i^{a,u} m_i^{a,u} - T p N_{\text{cell}} \ln C_1, \end{aligned} \quad (\text{A18})$$

where $p = 4$ denotes the size of the basis (sublattice). As a side note, the Lagrange multiplier \mathbf{A}_i^a can be interpreted as an effective mean field interacting with a local moment. Minimizing F_ρ , of Eq. A11, with respect to $m_i^{a,u}$ one has

$$A_i^{a,u} = \frac{\bar{h}_i^{a,u}}{T}, \quad (\text{A19})$$

where

$$\bar{h}_i^{a,u} = \sum_{j,b,v} \mathcal{J}_{uv}^{ab}(i,j) m_j^{b,v} + h_i^{a,u}, \quad (\text{A20})$$

is the u -th component of the effective field at site (i, a) . We next exploit the fact that the pyrochlore lattice has the underlying symmetry of a fcc lattice by defining the Fourier transforms,

$$m_i^{a,u} = \sum_{\mathbf{q}} m_{\mathbf{q}}^{a,u} e^{-i\mathbf{q} \cdot \mathbf{R}_i^a}, \quad (\text{A21})$$

$$\mathcal{J}_{uv}^{ab}(i, j) = \frac{1}{N_{\text{cell}}} \sum_{\mathbf{q}} \mathcal{J}_{uv}^{ab}(\mathbf{q}) e^{i\mathbf{q} \cdot \mathbf{R}_{ij}^{ab}}, \quad (\text{A22})$$

where N_{cell} is the number of fcc Bravais lattice points, but \mathbf{R}_i^a denotes the position of a spin. Equations A21 and A22 applied to F_ρ yield

$$\begin{aligned} \mathcal{F}_\rho(T) &= \frac{1}{2} \sum_{\mathbf{q}} \sum_{a,b} \sum_{u,v} m_{\mathbf{q}}^{a,u} (nT \delta^{a,b} \delta^{u,v} - \mathcal{J}_{uv}^{ab}(\mathbf{q})) m_{-\mathbf{q}}^{b,v} \\ &- \sum_{\mathbf{q}} \sum_{a,b} \sum_{u,v} \delta^{a,b} \delta^{u,v} h_{\mathbf{q}}^{a,u} m_{-\mathbf{q}}^{a,u} - T p \ln C_1, \end{aligned} \quad (\text{A23})$$

where $\mathcal{F}_\rho(T) = F_\rho(T)/N_{\text{cell}}$. A transformation to normal modes is necessary to diagonalize $\mathcal{J}_{uv}^{ab}(\mathbf{q})$. This is accomplished by the use of Eq. 9, or

$$m_{\mathbf{q}}^{a,u} = \sum_{\alpha=1}^4 \sum_{\mu=1}^3 U_{u,\mu}^{a,\alpha}(\mathbf{q}) \phi_{\mathbf{q}}^{\alpha,\mu}, \quad (\text{A24})$$

where the Greek indices (α, μ) label the normal modes. $U(\mathbf{q})$ is the unitary matrix that diagonalizes $\mathcal{J}(\mathbf{q})$ in the sublattice space with eigenvalues $\lambda(\mathbf{q})$,

$$U^\dagger(\mathbf{q}) \mathcal{J}(\mathbf{q}) U(\mathbf{q}) = \lambda(\mathbf{q}), \quad (\text{A25})$$

where in component form $U_{u,\mu}^{a,\alpha}(\mathbf{q})$ represents the (a, u) component of the (α, μ) eigenvector at \mathbf{q} with eigenvalue $\lambda_\mu^\alpha(\mathbf{q})$. The amplitudes of the normal modes are denoted by $\{\phi_{\mathbf{q}}\} = \{\sum_{\alpha,\mu} \phi_{\mathbf{q}}^{\alpha,\mu}\}$. Therefore, the MF free energy to quadratic order in the normal modes variables reads,

$$\begin{aligned} \mathcal{F}_\rho(T) &= \frac{1}{2} \sum_{\mathbf{q}} \sum_{\alpha,\mu} \phi_{\mathbf{q}}^{\alpha,\mu} (nT - \lambda_\mu^\alpha(\mathbf{q})) \phi_{-\mathbf{q}}^{\alpha,\mu} \\ &- T \sum_{\mathbf{q}} \sum_{\alpha,\mu} \tilde{h}_{\mathbf{q}}^{\alpha,\mu} \phi_{-\mathbf{q}}^{\alpha,\mu} - T p \ln C_1, \end{aligned} \quad (\text{A26})$$

where

$$\tilde{h}_{\mathbf{q}}^{\alpha,\mu} = \frac{1}{T} \sum_{a,u} h_{\mathbf{q}}^{a,u} U_{u,\mu}^{a,\alpha}(-\mathbf{q}).$$

Note that for the Ising case, the indices representing the spin components (u, v) and the corresponding modes (μ, ν) are dropped from Eq. A26.

The neutron scattering cross-section for unpolarized neutrons in the dipole approximation is given by Eq. 11^{65,66}, or

$$\frac{d\sigma(\mathbf{Q})}{d\Omega} = C [f(\mathbf{Q})]^2 \sum_{i,j} \sum_{a,b} \langle \mathbf{S}_{i\perp}^a \cdot \mathbf{S}_{j\perp}^b \rangle e^{i\mathbf{Q} \cdot \mathbf{R}_{ij}^{ab}}, \quad (\text{A27})$$

where \mathbf{Q} is the momentum transfer, i.e., $\mathbf{Q} = \mathbf{G} + \mathbf{q}$, \mathbf{G} is a fcc reciprocal lattice vector, \mathbf{q} is a wave vector in the first Brillouin zone, and C is a constant. The correlation function is between spin components perpendicular to the vector \mathbf{Q} ,

$$\begin{aligned} \langle \mathbf{S}_{i\perp}^a \cdot \mathbf{S}_{j\perp}^b \rangle &= \sum_{u,v} (\hat{n}_\perp^u \cdot \hat{n}_\perp^v) \langle S_i^{a,u} S_j^{b,v} \rangle \\ &= \sum_{u,v} \left(\delta^{u,v} - \frac{Q^u Q^v}{|\mathbf{Q}|^2} \right) \langle S_i^{a,u} S_j^{b,v} \rangle, \end{aligned} \quad (\text{A28})$$

where $\hat{n}_\perp^u = \hat{n}^u - (\hat{n}^u \cdot \hat{Q}) \hat{Q}$ is strictly a geometric factor and $\hat{Q} = \mathbf{Q}/|\mathbf{Q}|$. For Ising spins one replaces \hat{n}^u with \hat{z}^a from Table I and $S_i^{a,u}$ with σ_i^a . In order to proceed, the correlation function between spin variables, $\langle \mathbf{S}_{i\perp}^a \cdot \mathbf{S}_{j\perp}^b \rangle$, must be transformed to \mathbf{q} -space by use of Eq. A21 and then to normal mode variables by application of Eq. A24, one arrives at

$$\begin{aligned} \langle \mathbf{S}_{i\perp}^a \cdot \mathbf{S}_{j\perp}^b \rangle &= \sum_{\mathbf{q}, \mathbf{q}'} \sum_{\alpha, \beta} \sum_{\mu, \nu} \langle \phi_{\mathbf{q}}^{\alpha,\mu} \phi_{\mathbf{q}'}^{\beta,\nu} \rangle \\ &\times U_{u,\mu}^{a,\alpha}(\mathbf{q}) U_{v,\nu}^{b,\beta}(\mathbf{q}') e^{-i\mathbf{q} \cdot \mathbf{R}_i^a - i\mathbf{q}' \cdot \mathbf{R}_j^b}. \end{aligned} \quad (\text{A29})$$

The correlation function $\langle \phi_{\mathbf{q}}^{\alpha,\mu} \phi_{\mathbf{q}'}^{\beta,\nu} \rangle$ can be calculated from a partition function defined in terms of the normal mode amplitudes. The general definition reads,

$$Z = \text{Tr} \{ e^{-\mathcal{F}_\rho(T)/T} \}, \quad (\text{A30})$$

where $\mathcal{F}_\rho(T)$ is given by Eq. A26, and the trace is over all values of the normal mode amplitudes,

$$\text{Tr} \equiv \int_{-\infty}^{\infty} \prod_{\mathbf{q}, \alpha, \mu} d\phi_{\mathbf{q}}^{\alpha,\mu},$$

so one has,

$$Z = \prod_{\mathbf{q}, \alpha, \mu} \int_{-\infty}^{\infty} d\phi_{\mathbf{q}}^{\alpha,\mu} e^{-\frac{1}{2} (n - \frac{\lambda_\mu^\alpha(\mathbf{q})}{T}) |\phi_{\mathbf{q}}^{\alpha,\mu}|^2 + \tilde{h}_{\mathbf{q}}^{\alpha,\mu} \phi_{-\mathbf{q}}^{\alpha,\mu}}, \quad (\text{A31})$$

where a constant term has been dropped. The integral above is recast as a general Gaussian,

$$\int_{-\infty}^{\infty} d\phi e^{-\frac{1}{2} A \phi^2 + B \phi} = \sqrt{\frac{2\pi}{A}} e^{\frac{B^2}{2A}}, \quad (\text{A32})$$

where $A = (n - \frac{\lambda_\mu^\alpha(\mathbf{q})}{T})$ and $B = \tilde{h}_{\mathbf{q}}^{\alpha,\mu}$. Therefore, the final form of the partition function is,

$$\begin{aligned} Z &= \prod_{\mathbf{q}, \alpha, \mu} Z^{\alpha,\mu}(\mathbf{q}) \\ &= \prod_{\mathbf{q}, \alpha, \mu} \left[\frac{2\pi}{n - \frac{\lambda_\mu^\alpha(\mathbf{q})}{T}} \right]^{(1/2)} e^{(\tilde{h}_{\mathbf{q}}^{\alpha,\mu})^2 / 2(n - \lambda_\mu^\alpha(\mathbf{q})/T)}. \end{aligned} \quad (\text{A33})$$

The correlation function is now determined from derivatives of Z with respect to the fields $\tilde{h}_{\mathbf{q}}^{\alpha,\mu}$,

$$\begin{aligned} \langle \phi_{\mathbf{q}}^{\alpha,\mu} \phi_{\mathbf{q}'}^{\beta,\nu} \rangle &= \frac{1}{Z} \frac{\partial^2 Z}{\partial \tilde{h}_{\mathbf{q}}^{\alpha,\mu} \partial \tilde{h}_{\mathbf{q}'}^{\beta,\nu}} \Big|_{\tilde{h}_{\mathbf{q}}=0} \quad (\text{A34}) \\ &= \frac{\delta_{\mathbf{q}+\mathbf{q}',0} \delta^{\alpha,\beta} \delta^{\mu,\nu}}{\left(n - \frac{\lambda_{\mu}^{\alpha}(\mathbf{q})}{T}\right)}. \end{aligned}$$

Back substitution of the result from Eq. A34, into Eq. A29, then into Eq. A27, and finally imposing the properties of the Kronecker delta functions leaves

$$\begin{aligned} \frac{1}{N_{\text{cell}}} \frac{d\sigma(Q)}{d\Omega} &= C [f(Q)]^2 \sum_{\alpha,\mu} \sum_{a,b} \sum_{u,v} \frac{(\hat{n}_{\perp}^u \cdot \hat{n}_{\perp}^v)}{(n - \lambda_{\mu}^{\alpha}(\mathbf{q})/T)} \\ &\times U_{u,\mu}^{a,\alpha}(\mathbf{q}) U_{v,\nu}^{b,\beta}(-\mathbf{q}) e^{i\mathbf{G} \cdot \mathbf{r}^{ab}}, \quad (\text{A35}) \end{aligned}$$

where we have used the identity

$$\sum_{i,j} e^{i(\mathbf{Q}-\mathbf{q}) \cdot \mathbf{R}_{i,j}} e^{i(\mathbf{Q}-\mathbf{q}) \cdot \mathbf{r}^{ab}} = N_{\text{cell}} e^{i\mathbf{G} \cdot \mathbf{r}^{ab}}.$$

We find it convenient to define the function,

$$\begin{aligned} \mathbf{F}_{\mu,\perp}^{\alpha}(\mathbf{q}) &= \sum_{a,u} \hat{n}_{\perp}^u U_{u,\mu}^{a,\alpha}(\mathbf{q}) e^{i\mathbf{G} \cdot \mathbf{r}^a} \quad (\text{A36}) \\ &= \sum_a \left\{ U_{\mu}^{a,\alpha}(\mathbf{q}) - (U_{\mu}^{a,\alpha}(\mathbf{q}) \cdot \hat{Q}) \hat{Q} \right\} e^{i\mathbf{G} \cdot \mathbf{r}^a}, \end{aligned}$$

where $U_{\mu}^{a,\alpha}(\mathbf{q}) = \sum_u \hat{n}_{\perp}^u U_{u,\mu}^{a,\alpha}(\mathbf{q})$ (and therefore $\mathbf{F}_{\mu,\perp}^{\alpha}(\mathbf{q})$) is a three component vector. The scattering cross-section is written compactly as

$$\frac{1}{N_{\text{cell}}} \frac{d\sigma(Q)}{d\Omega} = C [f(Q)]^2 \sum_{\alpha,\mu} \frac{|\mathbf{F}_{\mu,\perp}^{\alpha}(\mathbf{q})|^2}{(n - \lambda_{\mu}^{\alpha}(\mathbf{q})/T)}, \quad (\text{A37})$$

which is Eq. 16 with $n = 3$. When considering $\langle 111 \rangle$ Ising spins, the arguments that follow Eq. A29 still hold, but the indices for the spin components (u, v) and corresponding normal modes (μ, ν) are dropped from the equations. The final expression for the scattering cross-section reads,

$$\frac{1}{N_{\text{cell}}} \frac{d\sigma(Q)}{d\Omega} = C [f(Q)]^2 \sum_{\alpha} \frac{|\mathbf{F}_{\perp}^{\alpha}(\mathbf{q})|^2}{(1 - \lambda^{\alpha}(\mathbf{q})/T)}, \quad (\text{A38})$$

where $\mathbf{F}_{\perp}^{\alpha}(\mathbf{q})$ is a three component vector given by,

$$\mathbf{F}_{\perp}^{\alpha}(\mathbf{q}) = \sum_a \hat{z}_{\perp}^a U^{a,\alpha}(\mathbf{q}) e^{i\mathbf{G} \cdot \mathbf{r}^a}, \quad (\text{A39})$$

which is just Eq. 18. We note that Eqs. A37 and A38 are only valid for $T > \lambda_{\mu}^{\alpha}(\mathbf{q}_{\text{ord}})/n$, where $\lambda_{\mu}^{\alpha}(\mathbf{q}_{\text{ord}}) = \max_{\mathbf{q}} \{\lambda^{\max}(\mathbf{q})\}$ is the critical eigenvalue, a global maximum, which sets T_c^{MF} and defines the paramagnetic regime. We also point out that the lattice structure and spin symmetry are contained in the respective $\mathbf{F}_{\perp}^{\alpha}(\mathbf{q})$ -functions, Eqs. A36 and A39; these properties will be exploited in Appendix D when we discuss symmetry allowed scattering patterns for Heisenberg and Ising spins.

1. Comment on the convention for the Fourier transform

Another convention for defining Fourier modes uses the Bravais lattice points, \mathbf{R}_i , in the definitions⁷⁶,

$$m_i^{a,u} = \sum_{\mathbf{q}} m_{\mathbf{q}}^{a,u} e^{-i\mathbf{q} \cdot \mathbf{R}_i}, \quad (\text{A40})$$

and

$$\mathcal{J}_{uv}^{ab}(i, j) = \frac{1}{N_{\text{cell}}} \sum_{\mathbf{q}} \mathcal{J}_{uv}^{ab}(\mathbf{q}) e^{i\mathbf{q} \cdot \mathbf{R}_{i,j}}. \quad (\text{A41})$$

Hence, this convention differs from the one we employ by a simple phase factor, $\exp(i\mathbf{q} \cdot \mathbf{r}^{ab})$ for $\mathcal{J}_{uv}^{ab}(i, j)$. The two approaches are equally valid and yield the same results; however, there are a couple important differences in the above results when this alternate convention is used. First, the interaction matrix defined by the inverse of Eq. A41 has complex entries. For nearest neighbor interactions between sites $a = 1$ and $b = 2$, we have

$$\mathcal{J}_{uv}^{ab}(\mathbf{q}) = \mathcal{J}_{uv}^{1,2}(1 + e^{-i\mathbf{q} \cdot \mathbf{R}_{i,j}}), \quad (\text{A42})$$

where the factor of 1 arises because the sites $a = 1$ and $b = 2$ are in the same tetrahedral basis unit, i.e., $\mathbf{R}_{i,j} = \mathbf{0}$, but its symmetric equivalent has $\mathbf{R}_{i,j} \neq \mathbf{0}$. Next, the definition for the scattering cross-section, Eq. A27, holds, but the expression for the correlation function between normal mode variables, Eq. A29, contains the phase factor $\exp(-i\mathbf{q} \cdot \mathbf{R}_i - i\mathbf{q}' \cdot \mathbf{R}_j)$. Carrying the necessary steps through to an expression for scattering cross-section, one finds that the factor $\exp(i\mathbf{G} \cdot \mathbf{r}^a)$ in Eqs. A36 and A39 is replaced by $\exp(i\mathbf{Q} \cdot \mathbf{r}^a)$. Recall that momentum transfer and reciprocal lattice vector are related according to $\mathbf{Q} = \mathbf{G} + \mathbf{q}$. The presentation found in Refs. 43 and 59 (as noticed recently by Kadowaki et al.³⁷) unintentionally mixes these two conventions.

APPENDIX B: HIGH TEMPERATURE EXPANSION OF THE GAUSSIAN APPROXIMATION

We demonstrate that the equations for the neutron scattering cross-section obtained from MFT at the Gaussian level, Appendix A, can also be formulated via a high temperature series expansion (HTSE) to lowest order in $\beta \equiv 1/T$, where T is temperature in units of k_B . In contrast to VMFT, in a HTSE there is no appeal to any simplifying approximation that changes the character of the density matrix and imposes constraints that keep the internal energy, $\text{Tr}\{\rho H\}$, fixed. We follow our established convention of treating the general case of anisotropic Heisenberg spins while pointing out the specific differences for $\langle 111 \rangle$ Ising spins when needed. The starting point is the Heisenberg Hamiltonian of Eq. 1

$$H_H = -\frac{1}{2} \sum_{i,j} \sum_{a,b} \mathcal{J}_{uv}^{ab}(i, j) S_i^{a,u} S_j^{b,v} \quad (\text{B1})$$

where $\mathcal{J}_{uv}^{ab}(i, j)$ contains both spin and coordinate degrees of freedom and is defined by Eq. 5.

In the formula for the scattering cross-section, Eq.11, one must calculate the perpendicular correlation function,

$$\langle \mathbf{S}_{i\perp}^a \cdot \mathbf{S}_{j\perp}^b \rangle = \sum_{u,v} (\hat{n}_\perp^u \cdot \hat{n}_\perp^v) \langle S_i^{a,u} S_j^{b,v} \rangle, \quad (\text{B2})$$

which is just Eq. 12. We express the correlation function $\langle S_i^{a,u} S_j^{b,v} \rangle$ as a series expansion in cumulants⁷⁷,

$$\langle S_i^{a,u} S_j^{b,v} \rangle = \sum_{m=0}^{\infty} \frac{(-\beta)^m}{m!} \langle S_i^{a,u} S_j^{b,v} H_H^m \rangle_c, \quad (\text{B3})$$

where $\langle \dots \rangle$ represents a thermal average with respect to H_H and $\langle \dots \rangle_c$ represents the cumulant expansion of the spin operators and H_H . Cumulants are evaluated as a trace over the $T = 0$ states, $\langle \dots \rangle_0 = \text{Tr}\{\dots\} / \text{Tr}\{1\}$, where $\text{Tr}\{1\} = \tilde{N}$ is a normalization factor, $(4\pi)^N$ for Heisenberg spins and $(2)^N$ for Ising spins, N is the total number of sites in the lattice. Therefore, the correlation function to lowest order in β is

$$\langle S_i^{a,u} S_j^{b,v} \rangle \approx \langle S_i^{a,u} S_j^{b,v} \rangle_c - \beta \langle S_i^{a,u} S_j^{b,v} H_H \rangle_c + \dots \quad (\text{B4})$$

For both Heisenberg and Ising Hamiltonians, any non-zero contribution to the correlation function must have an even number of spin components per site (i.e., $(S_i^{a,u})^2$). The zeroth order term in β is obtained trivially,

$$\langle S_i^{a,u} S_j^{b,v} \rangle_c = \langle S_i^{a,u} S_j^{b,v} \rangle_o = (1/n) \delta_{i,j} \delta^{a,b} \delta^{u,v},$$

The first order contribution has two terms in the cumulant,

$$\langle S_i^{a,u} S_j^{b,v} H \rangle_c = \langle S_i^{a,u} S_j^{b,v} H \rangle_o - \langle S_i^{a,u} S_j^{b,v} \rangle_o \langle H \rangle_o,$$

but the second does not contribute because $\langle H \rangle_o \propto \langle S_l^{\tilde{a},\tilde{u}} S_m^{\tilde{b},\tilde{v}} \rangle_o = 0$, spins in the Hamiltonian can not be at the same site. The first term yields the result

$$\begin{aligned} \langle S_i^{a,u} S_j^{b,v} H \rangle_o &= -\frac{1}{2} \sum_{l,m} \sum_{\tilde{a},\tilde{b}} \sum_{\tilde{u},\tilde{v}} \mathcal{J}_{\tilde{u}\tilde{v}}^{\tilde{a}\tilde{b}}(i, j) \langle S_i^{a,u} S_j^{b,v} S_l^{\tilde{a},\tilde{u}} S_m^{\tilde{b},\tilde{v}} \rangle_o \\ &= -(1/n^2) \mathcal{J}_{uv}^{ab}(i, j). \end{aligned} \quad (\text{B5})$$

Therefore, Eq. B4 can be rewritten as

$$\langle S_i^{a,u} S_j^{b,v} \rangle \approx (1/n) \delta_{i,j} \delta^{a,b} \delta^{u,v} + (\beta/n^2) \mathcal{J}_{uv}^{ab}(i, j) \quad (\text{B6})$$

We obtain an expression for the scattering cross-section by substituting the result of Eq. B6 into Eq. B2, and then that result into Eq. 11; we use the identity $\mathbf{Q} = \mathbf{q} + \mathbf{G}$ and the definition of the Fourier transform of $\mathcal{J}_{uv}^{ab}(i, j)$, Eq. 8, to arrive at,

$$\begin{aligned} \frac{1}{N_{\text{cell}}} \frac{d\sigma(Q)}{d\Omega} &= (C/n) [f(Q)]^2 \sum_{a,b} \sum_{u,v} (\hat{n}_\perp^u \cdot \hat{n}_\perp^v) \quad (\text{B7}) \\ &\times \left(\delta^{a,b} \delta^{u,v} + \frac{\beta}{n} \mathcal{J}_{uv}^{ab}(\mathbf{q}) \right) e^{i\mathbf{G} \cdot \mathbf{r}^{ab}}, \end{aligned}$$

where C is a constant. The interaction matrix, $\mathcal{J}_{uv}^{ab}(\mathbf{q})$, in Eq. B7 is not diagonal. In order to calculate the differential cross-section for the pyrochlore lattice, or any lattice with a basis, we must diagonalize $\mathcal{J}_{uv}^{ab}(\mathbf{q})$. This is done with unitary matrix $U(\mathbf{q})$, or $U_{u,\mu}^{a,\alpha}(\mathbf{q})$ in component form. The first term on the right hand side of Eq. B7 follows directly from the definition of $U(\mathbf{q})$,

$$\sum_{\alpha,\mu} U_{u,\mu}^{a,\alpha}(\mathbf{q}) U_{v,\mu}^{b,\alpha}(-\mathbf{q}) = \mathbf{I} = \delta^{a,b} \delta^{u,v}, \quad (\text{B8})$$

where \mathbf{I} is the appropriate identity matrix. The transformation of the second term uses Eq. A25, and solves for $\mathcal{J}(\mathbf{q})$,

$$\mathcal{J}(\mathbf{q}) = U^\dagger(\mathbf{q}) \lambda(\mathbf{q}) U(\mathbf{q}).$$

In component form, we have

$$\mathcal{J}_{uv}^{ab}(\mathbf{q}) = \sum_{\alpha,\mu} \lambda_\mu^\alpha(\mathbf{q}) U_{u,\mu}^{a,\alpha}(\mathbf{q}) U_{v,\mu}^{b,\alpha}(-\mathbf{q}). \quad (\text{B9})$$

Using the results from Eqs. B8 and B9, the expression for the scattering cross-section becomes,

$$\begin{aligned} \frac{1}{N_{\text{cell}}} \frac{d\sigma(Q)}{d\Omega} &= (C/n) [f(Q)]^2 \sum_{\alpha,\mu} \sum_{a,b} \sum_{u,v} (\hat{n}_\perp^u \cdot \hat{n}_\perp^v) \\ &\times \left(1 + \frac{\beta}{n} \lambda_\mu^\alpha(\mathbf{q}) \right) U_{u,\mu}^{a,\alpha}(\mathbf{q}) U_{v,\mu}^{b,\alpha}(-\mathbf{q}) e^{i\mathbf{G} \cdot \mathbf{r}^{ab}} \end{aligned} \quad (\text{B10})$$

In the high temperature limit ($\beta \rightarrow 0$), one can write

$$\left(1 + \frac{\beta}{n} \lambda_\mu^\alpha(\mathbf{q}) \right) \approx \left(1 - \frac{\beta}{n} \lambda_\mu^\alpha(\mathbf{q}) \right)^{-1},$$

and the mean field result is recovered,

$$\frac{1}{N_{\text{cell}}} \frac{d\sigma(Q)}{d\Omega} = C [f(Q)]^2 \sum_{\alpha,\mu} \frac{|\mathbf{F}_{\mu,\perp}^\alpha(\mathbf{q})|^2}{(n - \beta \lambda_\mu^\alpha(\mathbf{q}))}, \quad (\text{B11})$$

where $\mathbf{F}_{\mu,\perp}^\alpha(\mathbf{q})$ is given by Eq. A36. For a $\langle 111 \rangle$ Ising model, the indices (u, v) and (μ, ν) are dropped from our presentation, $n = 1$, and $\mathbf{F}_\perp^\alpha(\mathbf{q})$ is given by Eq. A39.

APPENDIX C: EWALD EQUATIONS

Here we treat the dipole-dipole term in $\mathcal{J}(\mathbf{q})$ via the Ewald method⁷⁸. In MFT one works in the thermodynamic limit, so one has an infinite lattice sum. Within the Ewald approach, one recasts this infinite and conditionally convergent series as two finite absolutely convergent (rapidly converging) sums^{61,74}. The application of Ewald's ideas to the Fourier transformed dipole-dipole interaction is equivalent to the method of long wave lengths presented in Ref. 61.

The general expression of the Fourier transformed dipole-dipole lattice sum is

$$\mathcal{A}(\mathbf{q}) = \sum_i' \sum_{\substack{a,b \\ u,v}} \mathcal{A}_{uv}^{ab} e^{-i\mathbf{q} \cdot \mathbf{R}_{ij}^{ab}}, \quad (\text{C1})$$

where

$$\mathcal{A}_{uv}^{ab} = \frac{\hat{n}^u \cdot \hat{n}^v}{|\mathbf{R}_{ij}^{ab}|^3} - \frac{3(\hat{n}^u \cdot \mathbf{R}_{ij}^{ab})(\hat{n}^v \cdot \mathbf{R}_{ij}^{ab})}{|\mathbf{R}_{ij}^{ab}|^5}. \quad (\text{C2})$$

The conventions for indices and vectors are described in Section II, and $\mathcal{A}(\mathbf{q})$ is a 12×12 matrix. The sum \sum_i is over all \mathbf{R}_{ij}^{ab} except the terms $\mathbf{R}_{ij}^{ab} = \mathbf{0}$. To implement the Ewald method, we rewrite Eq. C2 in the following form⁶³,

$$\mathcal{A}_{uv}^{ab} = -(\hat{n}^u \cdot \nabla_x)(\hat{n}^v \cdot \nabla_x) \left\{ \frac{1}{|\mathbf{R}_{ij}^{ab} - \mathbf{x}|} \right\}_{\mathbf{x}=\mathbf{0}}. \quad (\text{C3})$$

Equation C3 is used in Eq. C1, and in terms of components one has,

$$\mathcal{A}_{uv}^{ab}(\mathbf{q}) = -(\hat{n}^u \cdot \nabla_x)(\hat{n}^v \cdot \nabla_x) \left\{ \sum_i' \frac{e^{-i\mathbf{q} \cdot \mathbf{R}_{ij}^{ab}}}{|\mathbf{R}_{ij}^{ab} - \mathbf{x}|} \right\}_{\mathbf{x}=\mathbf{0}}. \quad (\text{C4})$$

The goal of the Ewald method is to rewrite Eq. C4, a conditionally convergent series, as two absolutely convergent series, one in real space and the other in reciprocal space (k -space). We begin by writing the sum inside the brackets as a sum over all \mathbf{R}_{ij}^{ab} , the result is,

$$\begin{aligned} \mathcal{A}_{uv}^{ab}(\mathbf{q}) &= -(\hat{n}^u \cdot \nabla_x)(\hat{n}^v \cdot \nabla_x) \left\{ \sum_i' \frac{e^{-i\mathbf{q} \cdot \mathbf{R}_{ij}^{ab}}}{|\mathbf{R}_{ij}^{ab} - \mathbf{x}|} \right\}_{\mathbf{x}=\mathbf{0}} \\ &+ \delta^{ab}(\hat{n}^u \cdot \nabla_x)(\hat{n}^v \cdot \nabla_x) \left\{ \frac{1}{|\mathbf{x}|} \right\}_{\mathbf{x}=\mathbf{0}}. \end{aligned} \quad (\text{C5})$$

Next, the definition of a Gaussian integral (also a gamma function identity⁷⁹),

$$\frac{1}{|\mathbf{R}|} = \frac{2}{\sqrt{\pi}} \int_0^\infty e^{-t^2 R^2} dt,$$

is used rewrite the point source term, $1/|\mathbf{R}_{ij}^{ab} - \mathbf{x}|$, in Eq. C5. The Fourier transformed dipole-dipole lattice sum now reads,

$$\begin{aligned} \mathcal{A}_{uv}^{ab}(\mathbf{q}) &= -(\hat{n}^u \cdot \nabla_x)(\hat{n}^v \cdot \nabla_x) \int_0^\infty dt \frac{2}{\sqrt{\pi}} e^{-i\mathbf{q} \cdot \mathbf{x}} \\ &\times \left\{ \sum_i' e^{-t^2 |\mathbf{R}_{ij}^{ab} - \mathbf{x}|^2 - i\mathbf{q} \cdot (\mathbf{R}_{ij}^{ab} - \mathbf{x})} \right\}_{\mathbf{x}=\mathbf{0}} \\ &+ \delta^{ab}(\hat{n}^u \cdot \nabla_x)(\hat{n}^v \cdot \nabla_x) \left\{ \frac{1}{|\mathbf{x}|} \right\}_{\mathbf{x}=\mathbf{0}}. \end{aligned} \quad (\text{C6})$$

The integral in Eq. C6 is divided into two regions, $[0, \alpha]$ and $[\alpha, \infty)$. It is from this decomposition that the real

space ($[\alpha, \infty)$) and k -space ($[0, \alpha]$) series will arise. We note that the series resulting from the $[\alpha, \infty)$ integral will have a divergence at $\mathbf{R}_{ij}^{ab} = \mathbf{0}$, hence this term is treated separately. The range of integration is controlled by α ; it has units of inverse distance and will play the role of a convergence parameter in the final series. Equation C6 now reads,

$$\mathcal{A}_{uv}^{ab}(\mathbf{q}) = W_{uv}^{ab}(\mathbf{q}) + X_{uv}^{ab}(\mathbf{q}) + Y_{uv}^{ab}, \quad (\text{C7})$$

where

$$\begin{aligned} W_{uv}^{ab}(\mathbf{q}) &= -(\hat{n}^u \cdot \nabla_x)(\hat{n}^v \cdot \nabla_x) \int_0^\alpha dt \frac{2}{\sqrt{\pi}} e^{-i\mathbf{q} \cdot \mathbf{x}} \\ &\times \left\{ \sum_i' e^{-t^2 |\mathbf{R}_{ij}^{ab} - \mathbf{x}|^2 - i\mathbf{q} \cdot (\mathbf{R}_{ij}^{ab} - \mathbf{x})} \right\}_{\mathbf{x}=\mathbf{0}}, \end{aligned} \quad (\text{C8})$$

$$\begin{aligned} X_{uv}^{ab}(\mathbf{q}) &= -(\hat{n}^u \cdot \nabla_x)(\hat{n}^v \cdot \nabla_x) \int_\alpha^\infty dt \frac{2}{\sqrt{\pi}} e^{-i\mathbf{q} \cdot \mathbf{x}} \\ &\times \left\{ \sum_i' e^{-t^2 |\mathbf{R}_{ij}^{ab} - \mathbf{x}|^2 - i\mathbf{q} \cdot (\mathbf{R}_{ij}^{ab} - \mathbf{x})} \right\}_{\mathbf{x}=\mathbf{0}}, \end{aligned} \quad (\text{C9})$$

$$\begin{aligned} Y_{uv}^{ab} &= \delta^{ab}(\hat{n}^u \cdot \nabla_x)(\hat{n}^v \cdot \nabla_x) \\ &\left\{ \frac{1}{|\mathbf{x}|} - \frac{2}{\sqrt{\pi}} \int_\alpha^\infty e^{-t^2 |\mathbf{x}|^2} dt \right\}_{\mathbf{x}=\mathbf{0}}. \end{aligned} \quad (\text{C10})$$

We treat the expressions for $W_{uv}^{ab}(\mathbf{q})$, $X_{uv}^{ab}(\mathbf{q})$, and Y_{uv}^{ab} in succession.

For $W_{uv}^{ab}(\mathbf{q})$, the sum inside the brackets is a periodic function in \mathbf{x} . Therefore, it can be expressed as a Fourier series,

$$f(\mathbf{x}) = \sum_i e^{-t^2 |\mathbf{R}_{ij}^{ab} - \mathbf{x}|^2 - i\mathbf{q} \cdot (\mathbf{R}_{ij}^{ab} - \mathbf{x})} = \sum_{\mathbf{k}} g_{\mathbf{k}} e^{i\mathbf{k} \cdot \mathbf{x}}. \quad (\text{C11})$$

Solving for $g_{\mathbf{k}}$ one has

$$g_{\mathbf{k}=\mathbf{G}} = \frac{4\pi}{v} \frac{e^{-i\mathbf{G} \cdot \mathbf{r}^{ab}}}{|\mathbf{q} - \mathbf{G}|^3} F(z), \quad (\text{C12})$$

where \mathbf{G} is a reciprocal lattice vector, v is the volume of the unit cell,

$$F(z) = \int_0^\infty y \sin(y) e^{-z^2 y^2} dy = \frac{\sqrt{\pi}}{4z^3} e^{-1/4z^2} \quad (\text{C13})$$

and $z = t/|\mathbf{q} - \mathbf{G}|$ ⁸⁰. One now has the following identity for $f(\mathbf{x})$,

$$\begin{aligned} f(\mathbf{x}) &= \sum_i e^{-t^2 |\mathbf{R}_{ij}^{ab} - \mathbf{x}|^2 - i\mathbf{q} \cdot (\mathbf{R}_{ij}^{ab} - \mathbf{x})} \\ &= \frac{4\pi}{v} \sum_{\mathbf{G}} \frac{e^{-i\mathbf{G} \cdot (\mathbf{r}^{ab} - \mathbf{x})}}{|\mathbf{q} - \mathbf{G}|^3} F(z). \end{aligned} \quad (\text{C14})$$

Substituting Eq. C14 into Eq. C8, differentiating, and imposing the limit on \mathbf{x} yields,

$$\begin{aligned} W_{uv}^{ab}(\mathbf{q}) &= \frac{4\pi}{v} \sum_{\mathbf{G}} \frac{[\hat{n}^u \cdot (\mathbf{q} - \mathbf{G})][\hat{n}^v \cdot (\mathbf{q} - \mathbf{G})]}{|\mathbf{q} - \mathbf{G}|^3} e^{-i\mathbf{G} \cdot \mathbf{r}^{ab}} \\ &\times \frac{2}{\sqrt{\pi}} \int_0^\alpha dt F(t/|\mathbf{q} - \mathbf{G}|). \end{aligned} \quad (\text{C15})$$

The integral over $[0, \alpha]$ is readily performed by using the result from Eq. C13. Therefore, the reciprocal space sum in the Ewald decomposition reads,

$$W_{uv}^{ab}(\mathbf{q}) = \frac{4\pi}{v} \sum_{\mathbf{G}} \frac{[\hat{n}^u \cdot (\mathbf{q} - \mathbf{G})][\hat{n}^v \cdot (\mathbf{q} - \mathbf{G})]}{|\mathbf{q} - \mathbf{G}|^2} \times e^{-|\mathbf{q} - \mathbf{G}|^2/4\alpha^2} e^{-i\mathbf{G} \cdot \mathbf{r}^{ab}}, \quad (\text{C16})$$

where the sum is over all reciprocal lattice vectors \mathbf{G} . We note, however, the series for $W_{uv}^{ab}(\mathbf{q})$ has a non-analytic term at $\mathbf{G} = \mathbf{0}$ when at the zone center, $\mathbf{q} = \mathbf{0}$. This point is discussed below.

The expression for $X_{uv}^{ab}(\mathbf{q})$, Eq. C9, can be rearranged to obtain an identifiable integral. By reversing the sum and integral in Eq. C9 we obtain,

$$X_{uv}^{ab}(\mathbf{q}) = -(\hat{n}^u \cdot \nabla_x)(\hat{n}^v \cdot \nabla_x) \sum_i' e^{-i\mathbf{q} \cdot \mathbf{R}_{ij}^{ab}} \times \frac{2}{\sqrt{\pi}} \int_{\alpha}^{\infty} dt e^{-t^2 |\mathbf{R}_{ij}^{ab} - \mathbf{x}|^2} \Big|_{\mathbf{x}=\mathbf{0}}. \quad (\text{C17})$$

The integral in Eq. C17 can be expressed as a complementary error function⁷⁹,

$$\text{erfc}(z) = \frac{2}{\sqrt{\pi}} \int_z^{\infty} e^{-x^2} dx.$$

A final form for $X_{uv}^{ab}(\mathbf{q})$ is obtained by first applying the differential operators in Eq. C17, followed by taking the limit $\mathbf{x} \rightarrow 0$, and then integrating to get,

$$X_{uv}^{ab}(\mathbf{q}) = \sum_i' (S1_{uv}^{ab}(\mathbf{R}_{ij}^{ab}) - S2_{uv}^{ab}(\mathbf{R}_{ij}^{ab})) e^{-i\mathbf{q} \cdot \mathbf{R}_{ij}^{ab}}, \quad (\text{C18})$$

where

$$S1_{uv}^{ab}(\mathbf{R}_{ij}^{ab}) = (\hat{n}^u \cdot \hat{n}^v) \times \left\{ \frac{2\alpha}{\sqrt{\pi}} \frac{e^{-\alpha^2 |\mathbf{R}_{ij}^{ab}|^2}}{|\mathbf{R}_{ij}^{ab}|^2} + \frac{\text{erfc}(\alpha |\mathbf{R}_{ij}^{ab}|)}{|\mathbf{R}_{ij}^{ab}|^3} \right\}, \quad (\text{C19})$$

$$S2_{uv}^{ab}(\mathbf{R}_{ij}^{ab}) = (\hat{n}^u \cdot \mathbf{R}_{ij}^{ab})(\hat{n}^v \cdot \mathbf{R}_{ij}^{ab}) \times \left\{ \left[\frac{4\alpha^3}{\sqrt{\pi} |\mathbf{R}_{ij}^{ab}|^2} + \frac{6\alpha}{\sqrt{\pi} |\mathbf{R}_{ij}^{ab}|^4} \right] e^{-\alpha^2 |\mathbf{R}_{ij}^{ab}|^2} + \frac{3 \text{erfc}(\alpha |\mathbf{R}_{ij}^{ab}|)}{|\mathbf{R}_{ij}^{ab}|^5} \right\}. \quad (\text{C20})$$

Equations C18-C20 form the real space sum in the Ewald decomposition of the dipole-dipole interaction. Note that the sum in Eq. C18 is over all Bravais lattice displacement vectors \mathbf{R}_{ij} , with j fixed, except $\mathbf{R}_{ij} = \mathbf{0}$. Hence, the real space Ewald series is analytic everywhere.

In treating the singular terms in Eq. C10, one applies differential operators first to get,

$$Y_{uv}^{ab} = \lim_{\mathbf{x} \rightarrow \mathbf{0}} \delta^{ab} \times \left\{ -\frac{(\hat{n}^u \cdot \hat{n}^v)}{|\mathbf{x}|^3} + \frac{3(\hat{n}^u \cdot \mathbf{x})(\hat{n}^v \cdot \mathbf{x})}{|\mathbf{x}|^5} + (S1_{uv}^{ab}(\mathbf{x}) - S2_{uv}^{ab}(\mathbf{x})) \right\}, \quad (\text{C21})$$

where $S1_{uv}^{ab}(\mathbf{x})$ and $S2_{uv}^{ab}(\mathbf{x})$ are given by Eqs. C19 and C20, respectively, with \mathbf{R}_{ij}^{ab} replaced by \mathbf{x} . To evaluate the limit in Eq. C21, one expands the exponential function to $O(\mathbf{x}^2)$ and the complementary error function to order $O(\mathbf{x}^3)$. The result is the constant,

$$Y_{uv}^{ab} = -\frac{4\alpha^3}{3\sqrt{\pi}} (\hat{n}^u \cdot \hat{n}^v) \delta^{a,b}. \quad (\text{C22})$$

Collecting the results of Eqs. C16, C18-C20 and C22, we write the Ewald representation of the \mathbf{q} -dependent dipole-dipole interaction as,

$$\mathcal{A}_{uv}^{ab}(\mathbf{q}) = -\frac{4\alpha^3}{3\sqrt{\pi}} (\hat{n}^u \cdot \hat{n}^v) \delta^{a,b} + \frac{4\pi}{v} \sum_{\mathbf{G}} K_{uv}(\mathbf{q} - \mathbf{G}) e^{-|\mathbf{q} - \mathbf{G}|^2/4\alpha^2} e^{-i\mathbf{G} \cdot \mathbf{r}^{ab}} + \sum_i' (S1_{uv}^{ab}(\mathbf{R}_{ij}^{ab}) - S2_{uv}^{ab}(\mathbf{R}_{ij}^{ab})) e^{-i\mathbf{q} \cdot \mathbf{R}_{ij}^{ab}}, \quad (\text{C23})$$

where

$$K_{uv}(\mathbf{q} - \mathbf{G}) = \frac{[\hat{n}^u \cdot (\mathbf{q} - \mathbf{G})][\hat{n}^v \cdot (\mathbf{q} - \mathbf{G})]}{|\mathbf{q} - \mathbf{G}|^2} \quad (\text{C24})$$

In our derivation of the Ewald equations there is no reference to a specific lattice structure. Therefore, the Ewald results encapsulated in Eq. C23 hold for any lattice described by a set of translation vectors $\{\mathbf{R}_{ij}^{ab}\}$. Through the unit vectors \hat{n}^u (where local quantization axes can be treated by including a sublattice index, i.e., $\hat{n}^{a,u}$), the freedom to define the spin symmetry (e.g., Heisenberg, XY, Ising) has been ensured, too. For the work discussed in this article, we consider both Heisenberg and (111) Ising spins on the pyrochlore lattice. For Heisenberg spins, $\mathcal{A}_{uv}^{ab}(\mathbf{q})$ is calculated for all sublattices (a, b) and spin components (u, v) , the resulting $\mathcal{A}(\mathbf{q})$ is a 12×12 symmetric matrix contribution to $\mathcal{J}(\mathbf{q})$. For (111) Ising spins, the sums over spin components are dropped and the local quantization vectors are substituted, \hat{z}^a . One calculates $\mathcal{A}^{ab}(\mathbf{q})$ for all sublattices (a, b) , resulting in $\mathcal{A}(\mathbf{q})$ a symmetric 4×4 contribution to $\mathcal{J}(\mathbf{q})$. For each pyrochlore model, $\mathcal{A}(\mathbf{q})$ is determined at every \mathbf{q} -point in a mesh that covers the first Brillouin zone in the (hhl) -plane. These matrices are stored and then used in the formation of $\mathcal{J}(\mathbf{q})$ to calculate the neutron scattering cross-section, Eq. 16 or Eq. 18, for a specified set of interaction parameters (i.e., J, D, Δ, T). Because $\mathcal{A}(\mathbf{q})$ is calculated only for \mathbf{q} in the first zone, the term $\mathcal{K}_{uv}(\mathbf{q} - \mathbf{G})$ in Eq. C23 is ill defined at $\mathbf{q} = \mathbf{G} = (000)$. We discuss the small \mathbf{q} behavior of the Ewald equations below.

The parameter α used to divide the integral in Eq. C6 functions as a convergence parameter in the Ewald sums, Eq. C23. Although, the result of $\mathcal{A}_{uv}^{ab}(\mathbf{q})$ is independent of the value of α , in practice one chooses an α so that both real and reciprocal sums converge rapidly. Note that the convergence of the real space sum, Eqs. C18-C20, is enhanced by a large value for α , while the convergence of the reciprocal sum, Eq. C16, is improved for a small α .

In choosing a convergence parameter, we followed Ref. 62 and set $\alpha = \sqrt{\pi/v}$, where v is the volume of the unit cell. For a pyrochlore lattice defined in the rhombohedral basis with a cubic cell size of \bar{a} , we used $v = \bar{a}^3/4$. The real and reciprocal space sums converged at about the same rate for this value of α . We obtained similar results for $\mathcal{A}_{uv}^{ab}(\mathbf{q})$ using $\alpha = \sqrt{\pi/2v}$ and $\alpha = \sqrt{2\pi/v}$. Our Ewald results were checked by comparing the maximum eigenvalues of $\mathcal{A}(\mathbf{q})$ to those generated from a direct lattice sum of $\mathcal{A}(\mathbf{q})$ out to some cut-off distance r_c . Comparisons were done for the bcc and fcc lattices. We also performed tests of our Ewald equations for the pyrochlore lattice by calculating the soft-mode spectrum of $\mathcal{A}(\mathbf{q})$ in the spin ice regime. In Fig. 3, Ewald results along the (00 ℓ) direction in the first Brillouin zone are compared to calculations with the dipolar sum cut-off at different maximum separation distances r_c . The cut-off results approach the Ewald results as r_c increases. In Fig. 2, the soft-mode spectrum of $\mathcal{A}(\mathbf{q})$ in spin ice regime is plotted in the (hhl)-plane. This spectrum of eigenvalues agrees well with the spectrum generated from a direct lattice sum for $\mathcal{A}(\mathbf{q})$ with a cut-off distance of $r_c = 1000$, Fig. 6 in Ref. 36. As noted in Section III, the Ewald method eliminates the ripples in the soft-mode spectrum of $\mathcal{A}(\mathbf{q})$ by effectively taking the range of interaction to infinity.

The reciprocal space sum in Eq. C23 has a non-analytic term at the point $\mathbf{q} = (000)$ in the first Brillouin zone. If we consider the $\mathbf{G} = (000)$ contribution to Eq. C16, we have,

$$W_{uv}^{ab}(\mathbf{q}, \mathbf{G} = \mathbf{0}) = \frac{4\pi}{v} \frac{(\hat{n}^u \cdot \mathbf{q})(\hat{n}^v \cdot \mathbf{q})}{|\mathbf{q}|^2} e^{-|\mathbf{q}|^2/4\alpha^2}. \quad (\text{C25})$$

In the limit of small \mathbf{q} the exponential is expanded to yield,

$$W_{uv}^{ab}(\mathbf{q}, \mathbf{G} = \mathbf{0}) \approx \frac{4\pi}{v} \frac{(\hat{n}^u \cdot \mathbf{q})(\hat{n}^v \cdot \mathbf{q})}{|\mathbf{q}|^2} \left(1 - \frac{|\mathbf{q}|^2}{4\alpha^2}\right), \quad (\text{C26})$$

where in the limit $\mathbf{q} \rightarrow \mathbf{0}$ the value of

$$\frac{4\pi}{v} \frac{(\hat{n}^u \cdot \mathbf{q})(\hat{n}^v \cdot \mathbf{q})}{|\mathbf{q}|^2}$$

depends on the direction in which one approaches the zone center. The non-analytic term can be related to the macroscopic field of the dipoles and is shape dependent, see Section 30 in Ref. 61. We drop this term from our calculation to obtain a completely smooth spectrum all the way to (000). The physics of spin ice is not affected by this omission because all modes contribute to the PM scattering with (001) going critical at T_c^{MF} . The case of $\text{Tb}_2\text{Ti}_2\text{O}_7$ is more subtle because it is the (000) soft mode that goes critical. However, our focus here is not the order state of $\text{Tb}_2\text{Ti}_2\text{O}_7$, where a $\mathbf{q} = \mathbf{0}$ ordered state is expected for a pyrochlore AFM with either $\langle 111 \rangle$ Ising^{24,26,33} or Heisenberg⁵ spins. Instead, we are concerned with understanding the physics in the paramagnetic regime of this system as a first step toward unraveling the mystery surrounding the failure of $\text{Tb}_2\text{Ti}_2\text{O}_7$ to order at 50 mK.

APPENDIX D: SYMMETRY EXCLUDED SCATTERING

The paramagnetic neutron scattering spectrum of $\text{Tb}_2\text{Ti}_2\text{O}_7$ in the (hhl) plane contains a strong but broad region of intensity about (002) with no discernible correlations near the zone center, (000)⁴⁵. In this appendix, we put forward arguments based only on the structure of the lattice and the symmetry of spin space to demonstrate that the PM scattering intensity profile described above can not be realized by $\langle 111 \rangle$ Ising spins on the pyrochlore lattice but is allowed if the spins are Heisenberg like.

For the Ising pyrochlores, the map of scattering intensity is determined by the function $\mathbf{F}_\perp^\alpha(\mathbf{q})$, Eq. 19, which contains only information on the symmetry of the lattice through the eigenvectors, $U^{a,\alpha}(\mathbf{q})$, and the phase factor, $\exp(i\mathbf{G} \cdot \mathbf{r}^a)$, and the symmetry of spin space through the local quantization axis, \mathbf{z}^a . We consider a unit tetrahedron with scattering vectors \mathbf{Q} restricted to the (00 ℓ) direction. To handle the situation near the origin, we express all \mathbf{Q} as a small displacement from a reciprocal lattice vector, i.e., $\mathbf{Q} = \mathbf{G} + \mathbf{q} = (00\ell) + (00\delta)$, where $0 < \delta < 1$, ℓ is an integer, and a factor of $2\pi/\bar{a}$ is implied. The term (00 δ) falls in the first zone and, therefore, determines the eigenvalues and eigenvectors. Using the values for \mathbf{r}^a and \hat{z}^a defined in Table I we write,

$$\begin{aligned} \mathbf{F}_\perp^\alpha(00\ell + \delta) &= \frac{(1, 1, 0)}{\sqrt{3}} (U^{1,\alpha}(\delta) - U^{2,\alpha}(\delta)) \quad (\text{D1}) \\ &+ \frac{(1, -1, 0)}{\sqrt{3}} (U^{4,\alpha}(\delta) - U^{3,\alpha}(\delta)) e^{i\frac{\ell\pi}{2}}. \end{aligned}$$

Note that the projections of the spins onto the plane perpendicular to the direction of \mathbf{Q} sum to zero, (i.e., $\hat{z}_\perp^{(1)} + \hat{z}_\perp^{(2)} + \hat{z}_\perp^{(3)} + \hat{z}_\perp^{(4)} = 0$). For wave vectors $\mathbf{Q} = (00\delta)$ and $\mathbf{Q} = (002 + \delta)$ one has the following,

$$\begin{aligned} \mathbf{F}_\perp^\alpha(00\delta) &= \frac{(1, 1, 0)}{\sqrt{3}} (U^{1,\alpha}(\delta) - U^{2,\alpha}(\delta)) \quad (\text{D2}) \\ &+ \frac{(1, -1, 0)}{\sqrt{3}} (U^{4,\alpha}(\delta) - U^{3,\alpha}(\delta)), \end{aligned}$$

and

$$\begin{aligned} \mathbf{F}_\perp^\alpha(002 + \delta) &= \frac{(1, 1, 0)}{\sqrt{3}} (U^{1,\alpha}(\delta) - U^{2,\alpha}(\delta)) \quad (\text{D3}) \\ &- \frac{(1, -1, 0)}{\sqrt{3}} (U^{4,\alpha}(\delta) - U^{3,\alpha}(\delta)). \end{aligned}$$

The modulus squared of these two functions, e.g., the numerator of the scattering cross-section, yields the same numerical result,

$$\begin{aligned} |\mathbf{F}_\perp^\alpha(00\delta)|^2 &= |\mathbf{F}_\perp^\alpha(002 + \delta)|^2 \\ &= \frac{1}{3} \left\{ (U^{1,\alpha}(\delta) - U^{2,\alpha}(\delta) - U^{3,\alpha}(\delta) + U^{4,\alpha}(\delta))^2 \right. \\ &\quad \left. + (U^{1,\alpha}(\delta) - U^{2,\alpha}(\delta) + U^{3,\alpha}(\delta) - U^{4,\alpha}(\delta))^2 \right\}. \end{aligned}$$

This means the scattering cross-section, given by Eq. 18, in the limit $\delta \rightarrow 0$, is the same (or exactly correlated) for (000) and (002), absent the magnetic form factor ($f(Q)$). Therefore, the paramagnetic scattering of $\text{Tb}_2\text{Ti}_2\text{O}_7$ can not be generated by a model with Ising spins (infinite local $\langle 111 \rangle$ anisotropy).

In the case of Heisenberg spins with finite single-ion anisotropy, we consider the function $\mathbf{F}_{\mu,\perp}^\alpha(\mathbf{q})$ is given by Eq. 17. Again, restricting ourselves to wave vectors along the (00 l) direction, we have the general result

$$\mathbf{F}_{\mu,\perp}^\alpha(00l + \delta) = \mathbf{U}_{\mu,\perp}^{1,\alpha}(\delta) + \mathbf{U}_{\mu,\perp}^{2,\alpha}(\delta) + \left(\mathbf{U}_{\mu,\perp}^{3,\alpha}(\delta) + \mathbf{U}_{\mu,\perp}^{4,\alpha}(\delta) \right) e^{i\frac{4\pi}{2}l}, \quad (\text{D4})$$

where $\mathbf{U}_{\mu,\perp}^{a,\alpha}(\delta) = (U_{x,\mu}^{a,\alpha}(\delta), U_{y,\mu}^{a,\alpha}(\delta), 0)$. For \mathbf{Q} near (000) and (002), we obtain the following two forms,

$$\mathbf{F}_{\mu,\perp}^\alpha(00\delta) = \mathbf{U}_{\mu,\perp}^{1,\alpha}(\delta) + \mathbf{U}_{\mu,\perp}^{2,\alpha}(\delta) + \mathbf{U}_{\mu,\perp}^{3,\alpha}(\delta) + \mathbf{U}_{\mu,\perp}^{4,\alpha}(\delta), \quad (\text{D5})$$

and

$$\mathbf{F}_{\mu,\perp}^\alpha(002 + \delta) = \mathbf{U}_{\mu,\perp}^{1,\alpha}(\delta) + \mathbf{U}_{\mu,\perp}^{2,\alpha}(\delta) - \left(\mathbf{U}_{\mu,\perp}^{3,\alpha}(\delta) + \mathbf{U}_{\mu,\perp}^{4,\alpha}(\delta) \right). \quad (\text{D6})$$

Taking the modulus squared we get,

$$|\mathbf{F}_{\mu,\perp}^\alpha(00\delta)|^2 = (A^2 + B^2) + (C^2 + D^2) + 2(AC + BD), \quad (\text{D7})$$

and

$$|\mathbf{F}_{\mu,\perp}^{\alpha,\mu}(002 + \delta)|^2 = (A^2 + B^2) + (C^2 + D^2) - 2(AC + BD), \quad (\text{D8})$$

where

$$\begin{aligned} A &= U_{x,\mu}^{1,\alpha}(\delta) + U_{x,\mu}^{2,\alpha}(\delta), \\ B &= U_{y,\mu}^{1,\alpha}(\delta) + U_{y,\mu}^{2,\alpha}(\delta), \\ C &= U_{x,\mu}^{3,\alpha}(\delta) + U_{x,\mu}^{4,\alpha}(\delta), \\ D &= U_{y,\mu}^{3,\alpha}(\delta) + U_{y,\mu}^{4,\alpha}(\delta). \end{aligned} \quad (\text{D9})$$

Equations D7 and D8 are not strictly equivalent. Hence, it is possible to have paramagnetic spin-spin correlations about (002) while intensity about (000) is suppressed. This result puts on a firm theoretical footing the need to describe $\text{Tb}_2\text{Ti}_2\text{O}_7$ by a three-component Heisenberg model with finite anisotropy.

-
- * Electronic address: enjalran@gandalf.uwaterloo.ca
† Electronic address: gingras@gandalf.uwaterloo.ca
¹ A. P. Ramirez, *Annu. Rev. Mater. Sci.* **24**, 453 (1994).
² J. E. Greedan, *J. Mater. Chem.* **11**, 37 (2001).
³ S. T. Bramwell and M. J. P. Gingras, *Science* **294**, 1495 (2001).
⁴ N. P. Raju, M. Dion, M. J. P. Gingras, T. E. Mason, and J. E. Greedan, *Phys. Rev. B* **59**, 14 489 (1999).
⁵ S. E. Palmer and J. T. Chalker, *Phys. Rev. B* **62**, 488 (2000).
⁶ J. D. M. Champion, A. S. Wills, T. Fennell, S. T. Bramwell, J. S. Gardner, and M. A. Green, *Phys. Rev. B* **64**, 140407 (2001).
⁷ S. R. Dunsiger, R. F. Kiefl, K. H. Chow, B. D. Gaulin, M. J. P. Gingras, J. E. Greedan, A. Keren, K. Kojima, G. M. Luke, W. A. MacFarlane, et al., *Phys. Rev. B* **54**, 9019 (1996).
⁸ M. J. P. Gingras, C. V. Stager, N. P. Raju, B. D. Gaulin, and J. E. Greedan, *Phys. Rev. Lett.* **78**, 947 (1997).
⁹ J. S. Gardner, B. D. Gaulin, S. -H. Lee, C. Broholm, N. P. Raju, and J. E. Greedan, *Phys. Rev. Lett.* **83**, 211 (1999).
¹⁰ B. D. Gaulin, J. N. Reimers, T. E. Mason, J. E. Greedan, and Z. Tun, *Phys. Rev. Lett.* **69**, 3244 (1992).
¹¹ J. N. Reimers, J. E. Greedan, R. K. Kremer, E. Gmelin, and M. A. Subramanian, *Phys. Rev. B* **43**, 3387 (1991).
¹² M. J. Harris, S. T. Bramwell, D. F. McMorrow, T. Zeiske, and K. W. Godfrey, *Phys. Rev. Lett.* **79**, 2554 (1997).
¹³ A. P. Ramirez, A. Hayashi, R. J. Cava, R. Siddharthan, and B. S. Shastry, *Nature* **399**, 333 (1999).
¹⁴ B. S. Shastry, cond-mat/0210230, unpublished.
¹⁵ J. S. Gardner, S. R. Dunsiger, B. D. Gaulin, M. J. P. Gingras, J. E. Greedan, R. F. Kiefl, M. D. Lumsden, W. A. MacFarlane, N. P. Raju, J. E. Sonier, et al., *Phys. Rev. Lett.* **82**, 1012 (1999).
¹⁶ Y. Taguchi, Y. Oohara, H. Yoshizawa, N. Nagaosa, and Y. Tokura, *Science* **291**, 2573 (2001).
¹⁷ D. Yanagishima and Y. Maeno, *J. Phys. Soc. Jpn* **70**, 2880 (2001).
¹⁸ M. Hanawa, Y. Muraoka, T. Tayama, T. Sakakibara, J. Yamamura, and Z. Hiroi, *Phys. Rev. Lett.* **87**, 187001 (2001).
¹⁹ H. Sakai, K. Yoshimura, H. Ohno, H. Kato, S. Kambe, R. E. Walstedt, T. D. Matsuda, and Y. Haga, *J. Phys. Condens. Matter* **13**, L785 (2001).
²⁰ S. Kondo, D. C. Johnston, C. A. Swenson, F. Borsa, A. V. Mahajan, L. L. Miller, T. Gu, A. I. Goldman, M. B. Maple, D. A. Gajewski, et al., *Phys. Rev. Lett.* **78**, 3729 (1997).
²¹ S. -H. Lee, C. Broholm, T. H. Kim, W. Ratcliff, and S. -W. Cheong, *Phys. Rev. B* **84**, 3718 (2000).
²² S. -H. Lee, C. Broholm, W. Ratcliff, G. Gasparovic, Q. Huang, T. H. Kim, and S. -W. Cheong, *Nature* **418**, 856 (2002).
²³ S. Rosenkranz, A. P. Ramirez, A. Hayashi, R. J. Cava, R. Siddharthan, and B. S. Shastry, *J. Appl. Phys.* **87**, 5914 (2000).
²⁴ M. J. P. Gingras, B. C. den Hertog, M. Faucher, J. S. Gardner, S. R. Dunsiger, L. J. Chang, B. D. Gaulin, N. P. Raju, and J. E. Greedan, *Phys. Rev. B* **62**, 6496 (2000).
²⁵ S. Bramwell and M. J. Harris, *J. Phys.: Condens. Matter* **10**, L215 (1998).
²⁶ R. Moessner, *Phys. Rev. B* **57**, R5587 ((1998)).
²⁷ J. D. Bernal and R. H. Fowler, *J. Chem. Phys.* **1**, 515 (1933).

- ²⁸ L. Pauling, **57**, 2680 (1935).
- ²⁹ L. Pauling, *The Nature of the Chemical Bond* (Cornell University Press, Ithaca, NY, 1960).
- ³⁰ S. T. Bramwell, M. J. Harris, B. C. den Hertog, M. J. P. Gingras, J. S. Gardner, D. F. McMorrow, A. R. Wildes, A. L. Cornelius, J. D. M. Champion, R. G. Melko, et al., *Phys. Rev. Lett.* **87**, 047205 (2001).
- ³¹ A. L. Cornelius and J. S. Gardner, *Phys. Rev. B* **64**, 060406 (2001).
- ³² S. Bramwell, M. J. P. Gingras, and J. N. Reimers, *J. Appl. Phys.* **75**, 5523 (1994).
- ³³ B. C. den Hertog and M. J. P. Gingras, *Phys. Rev. Lett.* **84**, 3430 (2000).
- ³⁴ B. C. den Hertog, M. J. P. Gingras, S. T. Bramwell, and M. J. Harris, cond-mat/9912220, unpublished.
- ³⁵ R. G. Melko, B. C. den Hertog, and M. J. P. Gingras, *Phys. Rev. Lett.* **87**, 067203 (2001), R. G. Melko, thesis, University of Waterloo, Ontario, Canada.
- ³⁶ M. J. P. Gingras and B. C. den Hertog, *Can. J. Phys.* **79**, 1339 (2001).
- ³⁷ H. Kadowaki, Y. Ishii, K. Matsuhira, and Y. Hinatsu, *Phys. Rev. B* **65**, 144421 (2002).
- ³⁸ R. Siddharthan, B. S. Shastry, A. P. Ramirez, A. Hayashi, R. J. Cava, and S. Rosenkranz, *Phys. Rev. Lett.* **83**, 1854 (1999).
- ³⁹ R. Siddharthan, B. S. Shastry, and A. P. Ramirez, *Phys. Rev. B* **63**, 184412 (2001).
- ⁴⁰ J. S. Gardner, private communication.
- ⁴¹ G. Luo, S. T. Hess, and L. R. Corruccini, *Phys. Lett. A* **291**, 306 ((2001)).
- ⁴² J. Villain, *Z. Phys. B* **33**, 31 (1979).
- ⁴³ J. N. Reimers, A. J. Berlinsky, and A. -C. Shi, *Phys. Rev. B* **43**, 865 (1991).
- ⁴⁴ R. Moessner and J. T. Chalker, *Phys. Rev. Lett.* **80**, 2929 (1998).
- ⁴⁵ J. S. Gardner, B. D. Gaulin, A. J. Berlinsky, P. Waldron, S. R. Dunsiger, N. P. Raju, and J. E. Greedan, *Phys. Rev. B* **64**, 224416 (2001).
- ⁴⁶ Y. Yasui, M. Kanada, M. Ito, H. Harashina, M. Sato, H. Okumura, K. Kakurai, and H. Kadowaki, *J. Phys. Soc. Jpn.* **71**, 599 (2002).
- ⁴⁷ Y. -J. Kao, M. Enjalran, and M. J. P. Gingras, cond-mat/0207270, unpublished.
- ⁴⁸ R. Moessner and J. T. Chalker, *Phys. Rev. B* **58**, 12049 (1998).
- ⁴⁹ W. I. Kinney and W. P. Wolf, *J. Appl. Phys.* **50**, 2115 (1979).
- ⁵⁰ P. Schiffer, A. P. Ramirez, D. A. Huse, and A. J. Valentino, *Phys. Rev. Lett.* **73**, 2500 (1994).
- ⁵¹ P. Schiffer, A. P. Ramirez, D. A. Huse, P. L. Gammel, U. Yaron, D. J. Bishop, and A. J. Valentino, *Phys. Rev. Lett.* **74**, 2379 (1995).
- ⁵² O. A. Petrenko, D. McK. Paul, C. Ritter, T. Zeiske, and M. Yethiraj, *Physica B* **266**, 41 (1999).
- ⁵³ O. A. Petrenko, C. Ritter, M. Yethiraj, and D. McK. Paul, *Phys. Rev. Lett.* **80**, 4570 (1998).
- ⁵⁴ A. P. Ramirez, private communication.
- ⁵⁵ A. P. Ramirez, B. S. Shastry, A. Hayashi, J. J. Krajewski, D. A. Huse, and R. J. Cava, *Phys. Rev. Lett.* **89**, 067202 (2002).
- ⁵⁶ J. A. Hodges, P. Bonville, A. Forget, A. Yaouanc, P. D. de Réotier, G. André, M. Rams, K. Królas, C. Ritter, P. C. M. Gubbens, et al., *Phys. Rev. Lett.* **88**, 077204 (2002).
- ⁵⁷ P. M. Chaikin and T. C. Lubensky, *Principles of Condensed Matter Physics* (Cambridge University Press, Cambridge, UK, 1995).
- ⁵⁸ A. B. Harris, O. G. Mouritsen, and A. J. Berlinsky, *Can. J. Phys.* **62**, 915 (1984).
- ⁵⁹ J. N. Reimers, *Phys. Rev. B* **46**, 193 (1992).
- ⁶⁰ M. Kanada, Y. Yasui, Y. Kondo, S. Iikubo, M. Ito, H. Harashina, M. Sato, H. Okumura, K. Kakurai, and H. Kadowaki, *J. Phys. Soc. Jpn.* **71**, 313 (2002).
- ⁶¹ M. Born and K. Huang, *Dynamical Theory of Crystal Lattices* (Oxford University Press, London, 1968).
- ⁶² M. H. Cohen and F. Keffer, *Phys. Rev.* **99**, 1128 (1955).
- ⁶³ A. Aharony and M. E. Fisher, *Phys. Rev. B* **8**, 3323 (1973).
- ⁶⁴ L. M. Holmes, J. Als-Nielsen, and H. J. Guggenheim, *Phys. Rev. B* **12**, 180 (1975).
- ⁶⁵ J. Jensen and A. R. MacKintosh, *Rare Earth Magnetism: Structures and Excitations* (Oxford University Press, New York, 1991).
- ⁶⁶ S. Lovesey, *Theory of neutron scattering from condensed matter*, vol. 2: Polarization effects and magnetic scattering of *International series of monographs on physics no. 72* (Oxford University Press, New York, 1984).
- ⁶⁷ R. G. Melko, M. Enjalran, B. C. den Hertog, and M. J. P. Gingras, unpublished.
- ⁶⁸ T. Fennell, O. A. Petrenko, G. Balakrishnan, S. T. Bramwell, J. D. M. Champion, B. Fåk, M. J. Harris, and D. McK. Paul, cond-mat/0107414, (unpublished).
- ⁶⁹ Mean-field calculations of the PM scattering at $r_c = 5, 10, 15$ with nearest neighbor exchange taken from Ref. 39, $J_{nn} = -1.90K$, are the same as displayed in Fig. 4, where $J_{nn} = -1.56/3 = -0.52K$.
- ⁷⁰ H. Fukazawa, R. G. Melko, R. Higashinaka, Y. Maeno, and M. J. P. Gingras, *Phys. Rev. B* **65**, 054410 (2002).
- ⁷¹ H. E. Viertiö and A. S. Oja, *Phys. Rev. B* **48**, 1062 (1993).
- ⁷² M. T. Heinilö and A. S. Oja, *Phys. Rev. B* **48**, 7227 (1993).
- ⁷³ B. Canals and D. A. Garanin, *Can. J. Phys.* **79**, 1323 (2001).
- ⁷⁴ S. L. de Leeuw, J. W. Perram, and E. R. Smith, *Proc. R. Soc. Lond. A* **373**, 27 (1980).
- ⁷⁵ S. R. Dunsiger, J. S. Gardner, J. A. Chakhalian, A. L. Cornelius, M. Jaime, R. F. Kiefl, R. Movshovich, W. A. MacFarlane, R. I. Miller, J. E. Sonier, et al., *Phys. Rev. Lett.* **85**, 3504 (2000).
- ⁷⁶ J. Schweizer, in *Neutron and Synchrotron Radiation for Condensed Matter Studies*, edited by J. Baruchel, J. L. Hodeau, M. S. Lehmann, J. R. Regnard, and C. Schlenker (Springer-Verlag, Berlin Heidelberg, 1994), vol. Vol II, p. 97.
- ⁷⁷ G. S. Rushbrooke, G. A. Baker, and P. J. Wood, *Phase Transitions and Critical Phenomena* (Academic Press, London New York, 1974), vol. 3, chap. Heisenberg Model, p. 245.
- ⁷⁸ P. P. Ewald, *Ann. Physik* **64**, 253 (1921).
- ⁷⁹ G. Arfken, *Mathematical Methods for Physicists* (Academic Press, San Diego, 1985), 3rd ed.
- ⁸⁰ The result of Eq. C13 is found in I.S. Gradshteyn and I. M. Ryzhik, *Table of Integrals, Series, and Products*, (Academic Press, San Diego, 1980), Corrected and Enlarged Edition, integral 3.952-1, page 495.